# Future Changes in Tropical and Extratropical Cyclones Affecting Hokkaido and Their Related Precipitation Based on Large-Ensemble Climate Simulations

SHO KAWAZOE,[a] MASARU INATSU,[a,b] TOMOHITO J. YAMADA,[b,c] AND TSUYOSHI HOSHINO[d]

[a] *Faculty of Science, Hokkaido University, Sapporo, Japan*
[b] *Center for Natural Hazards Research, Hokkaido University, Sapporo, Japan*
[c] *Faculty of Engineering, Hokkaido University, Sapporo, Japan*
[d] *Civil Engineering Research Institute for Cold Region, Sapporo, Japan*

(Manuscript received 8 February 2022, in final form 22 November 2022)

ABSTRACT: This study investigates the impact of future climate warming on tropical cyclones (TC) and extratropical cyclones (ETC) using the database for Policy Decision-Making for Future Climate Change (d4PDF) large ensemble simulations. Cyclone tracking was performed using the neighbor enclosed area tracking algorithm (NEAT), and TC and ETCs were identified over the western North Pacific Ocean (WNP). For cyclone frequency, it was revealed that, although a slight underestimation of the total number of TCs and ETCs in both the WNP and near Hokkaido, Japan, exists, the d4PDF reproduced the spatial distribution of both TC and ETC tracks well when compared with observations/reanalysis. The 4-K warming scenarios derived from six different sea surface temperature warming patterns showed robust decreases in TC frequency in the tropical WNP and a slight reduction in ETCs near Japan. Next, precipitation characteristics for TCs or ETCs in the vicinity of Hokkaido were examined using 5-km-mesh regional climate ensemble simulations. Four representative cyclone locations near Hokkaido are identified using *K*-means clustering and revealed distinct precipitation characteristics between clusters, with higher TC-associated precipitation than ETC-associated precipitation and the heaviest precipitation in the southern portion of the prefecture. The 4-K warming scenarios revealed increased precipitation for all cyclone placements for both TCs and ETCs. Last, average cyclone intensity, translation speed, and size were examined. It was shown that TCs in future climates are more intense, propagate more slowly, and are smaller in terms of enclosed vorticity area as they approach Hokkaido. For ETCs, mean intensity does not change much; they travel slightly faster, and become smaller.

KEYWORDS: Extratropical cyclones; Storm tracks; Tropical cyclones; Storm environments

## 1. Introduction

A major contributor to extreme precipitation is the direct impacts of tropical cyclones (TC) and extratropical cyclones (ETC). Hokkaido, Japan (Fig. 1a), is situated in a region where TCs approach or, in rare cases, make landfall in the prefecture. For example, in 2016, three typhoons (Canthu, Mindulle, and Kompasu) made landfall in Hokkaido, and one typhoon (Lionrock) passed near Hokkaido (Nayak and Takemi 2020a), which resulted in one of the most catastrophic weather disasters in prefectural record. Many TCs ultimately weaken and transition to ETCs before approaching Hokkaido (Kitabatake 2011). In addition, although ETCs originating in midlatitude regions are less frequent and intense in warmer months than in colder months, ~5 ETCs propagate over or near Hokkaido every summer season, often intensifying as they move northward and eastward (Lee et al. 2020). Regardless of how ETCs develop, strong ETCs can be accompanied by heavy precipitation and strong winds that can also have major socioeconomic consequences. Given the high-impact events accompanying cyclonic weather systems, there is interest in determining how extreme precipitation may change in association with TCs and ETCs. This is important near Hokkaido, where TCs and ETCs produce over 80% of the total or extreme precipitation (e.g., precipitation exceeding the 99th percentile) throughout the year (Pfahl and Wernli 2012).

It is expected that extreme precipitation frequency and intensity will increase in future climates in Japan (Kimoto et al. 2005; Emori and Brown 2005; Utsumi et al. 2011; Iizumi et al. 2012; Yamada et al. 2014; Hatsuzuka and Sato 2019). For TC-associated extremes, there is a consensus among the scientific community that global warming will amplify TC-associated extreme precipitation events (Knutson et al. 2020). Pseudo–global warming experiments for TCs (typhoons) approaching Hokkaido showed increased precipitation in future climates (Kanada et al. 2017a; Nayak and Takemi 2020b), and similar conclusions are reached from various modeling studies of TCs throughout Japan (e.g., Watanabe et al. 2019). Many studies project a decrease in TC frequency in the western North Pacific Ocean (WNP) but an increase in strong TCs (Oouchi et al. 2006; Murakami et al. 2012; Tsuboki et al. 2015; Yamada et al. 2017; Yoshida et al. 2017). This may result in higher intensity rain events from individual TCs near Hokkaido, even if such events occur less often.

Unlike TCs that have been shown to exhibit strong thermodynamical and dynamical changes, changes in ETC-associated extreme precipitation are believed to be associated with changes

Supplemental information related to this paper is available at the Journals Online website: https://doi.org/10.1175/JAMC-D-22-0018.s1.

*Corresponding author*: Sho Kawazoe, kawazoe@sci.hokudai.ac.jp

DOI: 10.1175/JAMC-D-22-0018.1

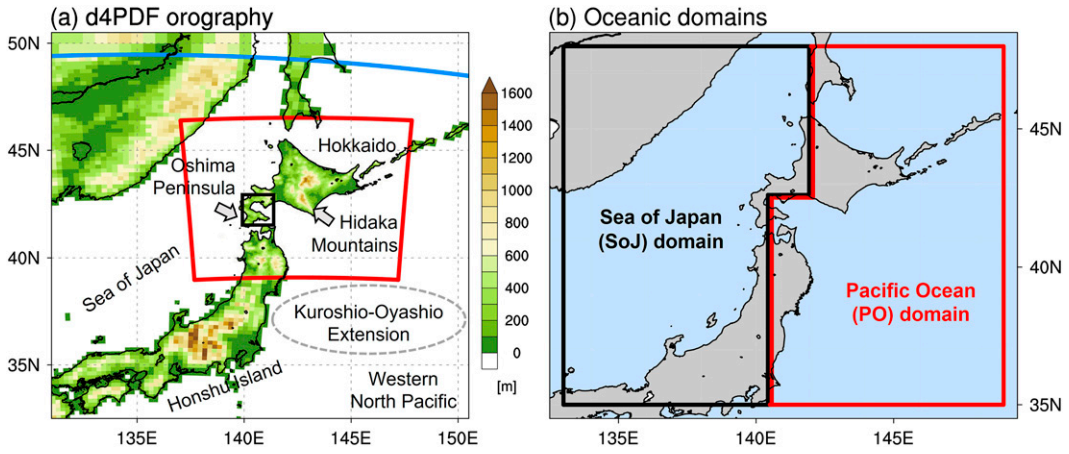


FIG. 1. (a) Model domains and orography (m). The blue line indicates the NHRCM20 domain, and the red line indicates the boundaries of the NHRCM05 domain. Shading represents elevation (m). (b) The SoJ (black outline) and PO (red outline) regions used to extract TC and ETCs.

mainly in the atmospheric moisture content. Previous modeling studies largely agree that warming temperatures will increase atmospheric moisture capacities, which will increase ETC-associated precipitation (Finnis et al. 2007). This signal is especially evident for the most intense ETCs (Hawcroft et al. 2018; Kodama et al. 2019), which generally produce the most intense precipitation events in the current climate (Hawcroft et al. 2012; Pfahl and Sprenger 2016). However, how ETCs will respond to changes in the background climate remains uncertain (Ulbrich et al. 2009; McDonald 2011; Catto et al. 2019). ETC intensity is highly dependent on low-level baroclinicity from the equator-to-pole temperature gradient, which is projected to weaken due to polar amplification. However, the projected strengthening of upper-level baroclinicity and increased latent heating due to increased atmospheric moisture can strengthen ETCs, possibly counteracting the effects of decreasing low-level baroclinicity. Many studies have indicated little change in future ETC intensity and therefore conclude that changes in precipitation are attributed primarily to increased moisture (Watterson 2006; Bengtsson et al. 2009; Michaelis et al. 2017; Yettella and Kay 2017; Sinclair et al. 2020; Priestley and Catto 2022).

To date, only a few studies have investigated future climate responses to TC and ETC-associated precipitation extremes in unison over Japan. Using satellite-based precipitation data, Utsumi et al. (2017) showed that the contribution of extreme daily precipitation between TCs and ETCs is similar (~40% each) for Japan. So, while TCs contribute to a larger fraction of extreme precipitation per storm, ETC passage occurs much more frequently. Hence, examining changes in both cyclonic weather systems together is worthwhile. In this study, we investigated widespread extreme precipitation events and their future changes in Hokkaido using a large ensemble of simulations from the database for Policy Decision-Making for Future Climate Change (d4PDF; Mizuta et al. 2017). We examine several characteristics of TCs and ETCs that influence heavy precipitation in Hokkaido, including moisture transport, cyclone intensity, translation speed, and size. Moisture transport was examined to understand how changes in the moisture and wind speeds within TCs and ETCs contribute to extreme precipitation. Changes in storm intensity have probably received the most attention in identifying warming scenario responses, as intense cyclones have been well documented as sources of widespread weather disasters, which may be exacerbated by a warming climate. Changes to TC translation speeds have received considerable interest in recent years (Kossin 2018; Chan 2019; Moon et al. 2019; Zhang et al. 2020), as the damaging impacts of slow-moving TCs have naturally led to an increase in studies examining their future changes (Gutmann et al. 2018; Yamaguchi and Maeda 2020; Yamaguchi et al. 2020). Last, cyclone size is critical in understanding total damage potential (Powell and Reinhold 2007), and projected changes in TC size in warming scenarios provide valuable information. While these papers focus on TC characteristics, it can be argued that ETCs may have similar responses to a warming climate, and a greater number of future ETCs could have similar impacts to weaker TCs in the current climate.

## 2. Data and methods

### a. Experimental design

We used historical and future climate simulations from the d4PDF large ensemble dataset. The d4PDF consists of the 60-km-mesh global simulation ensemble from the Meteorological Research Institute atmospheric general circulation model 3.2 (MRI-ACGCM; Mizuta et al. 2012) and the dynamically downscaled regional simulation covering Japan and eastern portions of the Asian continent using the 20-km-mesh Nonhydrostatic Regional Climate Model (NHRCM20; Sasaki et al. 2011), with each simulation containing 60 years (1951–2010) of historical (HIST) and a 4-K warming scenario (+4-K) simulation. One hundred MRI-AGCM ensemble members for the HIST climate were created using different initial conditions and small sea surface temperature (SST) perturbations arising

from analysis errors in observed monthly SSTs and sea ice concentration from the Centennial Observation-Based Estimates of SST, version 2 (COBE-SST2; Hirahara et al. 2014). Initial conditions were extracted from different time steps from a previous MRI-AGCM3.2 simulation. The +4-K represents a climate that is 4-K warmer relative to preindustrial levels, corresponding to a climate around the year 2090 under phase 5 of the Coupled Model Intercomparison Project (CMIP5) representative concentration pathway 8.5 scenario. Ninety ensemble members were created by adding SST warming patterns (ΔSST) from six CMIP5 simulations to detrended monthly SSTs from COBE-SST2. The six CMIP5 models used are the Community Climate System Model, version 4 (CCSM4); the Geophysical Fluid Dynamics Laboratory Climate Model, version 3 (GFDL-CM3); the Hadley Centre Global Environmental Model, version 2, atmosphere–ocean (HadGEM2-AO); the Model for Interdisciplinary Research on Climate, version 5 (MIROC5); the Max Planck Institute Earth System Model, medium resolution (MPI-ESM-MR); and the Meteorological Research Institute Coupled Atmosphere–Ocean General Circulation Model, version 3 (MRI-CGCM3). These models are determined through cluster analysis (Mizuta et al. 2014) as an adequate representation of most of the uncertainty present in the SST change distributions for all CMIP5 models. The NHRCM20 product, which is not directly used for this study, offers 50 ensembles for HIST and 90 ensembles for +4-K. For further details and previous research examples utilizing d4PDF, we refer the reader to Mizuta et al. (2017) and a comprehensive review paper by Ishii and Mori (2020).

Further dynamical downscaling from NHRCM20 to 5-km horizontal grid spacing (NHRCM05) covering northern Japan (Fig. 1a) is also used for this study. Because of the large computational demand, downscaling was performed for the entire year (starting in August) only if they featured the top several hundred annual maximum 72-h cumulative rainfall events in the Tokachi River basin (south-central Hokkaido) from the 3000-yr HIST and 5400-yr +4-K NHRCM20 ensemble. Further details can be found in Hoshino et al. (2020) and Yamada et al. (2021). For our study, precipitation data from 769-yr HIST and 735-yr +4-K are examined.

### b. Observations and reanalysis

To evaluate the model reproducibility of TC track density and appropriately adjust our tracking algorithm parameters to reproduce observational TC frequency, we used the Regional Specialized Meteorological Center Tokyo-Typhoon Center Best Track Data (hereinafter BestTrack). Tracks from 1979 to 2010 were used, and tracks with tropical storm intensity or greater (>17 m $s^{-1}$) were used as guidance for tracking parameter adjustment. Because there are no observed ETC datasets, the Japanese 55-year Reanalysis (JRA-55; Kobayashi et al. 2015; Harada et al. 2016) and the European Centre for Medium-Range Weather Forecasts fifth-generation atmospheric reanalysis (ERA5; Hersbach et al. 2020) were used to extract ETCs. The 55-km JRA-55 and 31-km ERA5 datasets from 1979 to 2010 were regridded to the same 60-km horizontal grid as the MRI-AGCM.

To validate NHRCM05 precipitation, the Radar/Rain Gauge-Analyzed Precipitation (RA) dataset between 2006 and 2019 was used. The current version (since 2006) of the RA is based on 46 C-band radars administered by both the Japan Meteorological Agency (JMA) and the Ministry of Land and Infrastructure, Transport and Tourism, which are combined with more than 10 000 rain gauge stations to produce an areal precipitation dataset covering the Japanese archipelago (Ishizaki and Matsuyama 2018). Data were provided as hourly accumulations on a 1-km horizontal grid. We regridded the RA to the same 5-km grid as the NHRCM05 for comparison using a first-order conservative mapping procedure (Jones 1999) commonly used for precipitation regridding, which accounts for the fractional contribution of the 1-km input grid to the 5-km output grid.

### c. Cyclone tracking method

Cyclones are identified and tracked from 850-hPa relative vorticity using the neighbor enclosed area tracking (NEAT) algorithm (Inatsu 2009; Satake et al. 2013). Unlike conventional neighbor point tracking methods (NPT), where local maximum vorticity or sea level pressure (SLP) that exceeds some threshold is identified as a cyclone center point, NEAT searches for an enclosed area of vorticity that meets a threshold criterion and defines this entire area as a cyclone. Additionally, while NPT searches for a local vorticity maximum at each time step and tracks the cyclone if it is within a certain distance from the previous time step, NEAT tracking is based on the area of cyclone overlap in subsequent time steps. The tracks are identified using the centroid location of the enclosed area of vorticity and begin (genesis) and end (lysis) if there is no overlap between cyclones before or after a time step. As cyclones are identified based on an enclosed area, the NEAT algorithm produces supplementary cyclone characteristics such as cyclone size, merging and splitting cyclones, in addition to tracks, genesis, lysis, and translation speed that can be provided by the NPT method without the need for any postprocessing.

Using 6-hourly data from the JRA-55, ERA5, 50-member HIST, and 90-member +4-K, cyclones are first extracted using the following conditions, adopted from Inatsu (2009):

1) 850-hPa relative vorticity exceeds $8.0 \times 10^{-5}$ $s^{-1}$ [a nine-point smoother is applied before tracking; we omit any vorticity values from grid points greater than 1500-m elevation from the JRA-55/ERA5 (850-hPa winds from MRI-AGCM3.2 are not extrapolated below the surface)];
2) enclosed cyclone area exceeds 20 000 $km^2$ and overlap area between consecutive time steps that exceeds 10 000 $km^2$; and
3) lifetime duration of a cyclone is at least 36 h from cyclone genesis to lysis.

Once cyclones are extracted, we distinguish TCs and ETCs by the presence of a warm core. Many of the methods from Satake et al. (2013) were implemented, but with some additional

conditions and modifications to better reproduce characteristics from BestTrack:

1) temperature anomaly at 500 hPa is greater than 0.8 K and is located within 2° from the cyclone center (anomaly is defined as 500-hPa temperature deviations from the mean temperature over a 7° × 7° grid box surrounding the cyclone center);
2) inside the enclosed cyclone area, the maximum wind speed at 850 hPa is greater than the maximum wind speed at 300 hPa;
3) TC genesis is located south of 35°N and does not occur over land; and
4) the cyclone meets the above criteria for 36 h or longer (a single time step failure is allowed).

All storms not meeting TC criteria and persisting for 36 h or longer were identified as ETCs. These include cyclones that transition from TCs to ETCs, which are common for cyclones approaching Hokkaido. For such cases, the timeframes when cyclones are identified as ETCs are required to last at least 18 h after transition, and the first time step following the transition was removed to omit cyclones that resemble TCs rather than ETCs.

We recognize that the relative vorticity of $8.0 \times 10^{-5}$ s$^{-1}$ is a higher threshold for ETCs than the commonly used $1.0 \times 10^{-5}$ s$^{-1}$. However, since intense ETCs generally produce heavier precipitation and will likely see stronger responses to a warming climate, we opted to keep a singular threshold to identify both TCs and ETCs. In addition, the 3000+-yr large ensemble dataset allows for robust evaluation of future changes in ETCs without incorporating weaker cyclones that may have otherwise been needed for single ensemble modeling studies.

### d. *Identification of cyclones producing widespread extreme precipitation in Hokkaido*

To examine cyclones that produce widespread extreme precipitation events (WEP), we first extracted all 6-hourly time steps when NHRCM05 HIST precipitation exceeds a 1-yr return period (computed at each grid point) for at least 10% of the total land grid points over Hokkaido. This 10% threshold was chosen based on the ability to examine a robust enough sample size while still investigating extreme events, similar to methods used by Kawazoe and Gutowski (2018) and Tamaki et al. (2018). It also allows us to focus primarily on resolved synoptic patterns producing precipitation rather than smaller-scale convective storms. Next, we extracted all cyclones that enter a 10° × 10° grid box from the center of Hokkaido (approximately 43.5°N, 142.5°E) for all time steps exhibiting WEP. Last, we decomposed cyclones causing WEP into four clusters using *K*-means clustering, similar to previous studies (Miyasaka et al. 2020; Hatsuzuka and Sato 2022). We examined the precipitation distribution in Hokkaido for all cyclones that exhibit similar patterns, how they change in +4-K, and possible environmental mechanisms that result in these changes. We also examined the effects of 850-hPa moisture flux (MF850) and its convergence (MFC850) to determine their role in the precipitation distribution, if they differ between TCs and ETCs, and how they change under warming scenarios. Our focus is from July to November (JASON).

### e. *Cyclone characteristics*

Additional factors may also determine how impactful TC- and ETC-associated precipitation may become. Therefore, we examined cyclone intensity, translation speed, and size (area), of which the latter two are default outputs from NEAT. For intensity, minimum SLP within the enclosed cyclone area was used. The translation speed is the average scalar speed of the cyclone centroid between time steps.

For this analysis, we separated TCs and ETCs based on their location [the Sea of Japan (SoJ) and Pacific Ocean (PO) domains; Fig. 1b] to examine if there are different cyclone characteristics in different regions. As highlighted in Kitano et al. (2017), TCs approaching Hokkaido between 1961 and 2016 are dominated by those propagating over the SoJ, but those coming from the PO have weakened less rapidly, primarily due to less land interaction. In addition, TC tracks are heavily influenced by large-scale circulation patterns, with the WNP subtropical high (WNPSH) and mid- to upper-level flow being the dominant steering sources. The positioning of the high varies throughout the year, leading to differences in storm tracks for TCs approaching Japan. These environmental conditions may contribute to interbasin differences in response to climate change.

## 3. Results

### a. *Cyclone distribution and projected changes*

TC track density for JASON from BestTrack and MRI-AGCM are shown in Figs. 2a and 2b. The overall spatial distribution and annual track density are consistent between the two datasets. Several distinguishable characteristics include a higher number of tracks near the Philippines and a lower number of tracks from around the Ryukyu Islands (approximately 26°N–127°E) and northward toward mainland Japan in the MRI-AGCM. This may indicate that more TCs transition to ETCs earlier using our TC extraction method. This can be seen in TC tracks from the JRA-55 (Fig. S1a in the online supplemental material), as it also produces fewer TCs farther north than BestTrack. The ERA5 shows more TCs to the north (Fig. S1b) but is largely overestimated near the Philippines, indicating that while higher resolution yields more TCs, spatial biases persist. Adjusting the vorticity/area/overlap threshold in NEAT increased TC density mainly near the Philippines but without significant increases farther north. Table 1 shows the total number of TCs in the WNP and within the black and red regions in Fig. 1b. While models indicate a slight underestimation of TCs relative to BestTrack, adjusting the TC frequency for the MRI-AGCM/JRA-55/ERA5 to BestTrack again led to a disproportional increase in the tropical WNP but only slight increases in those approaching Hokkaido. Previous studies have shown that the onset of even weak to moderate shear may not weaken TCs immediately, with approximately a 36-h lag between shear onset and weakening

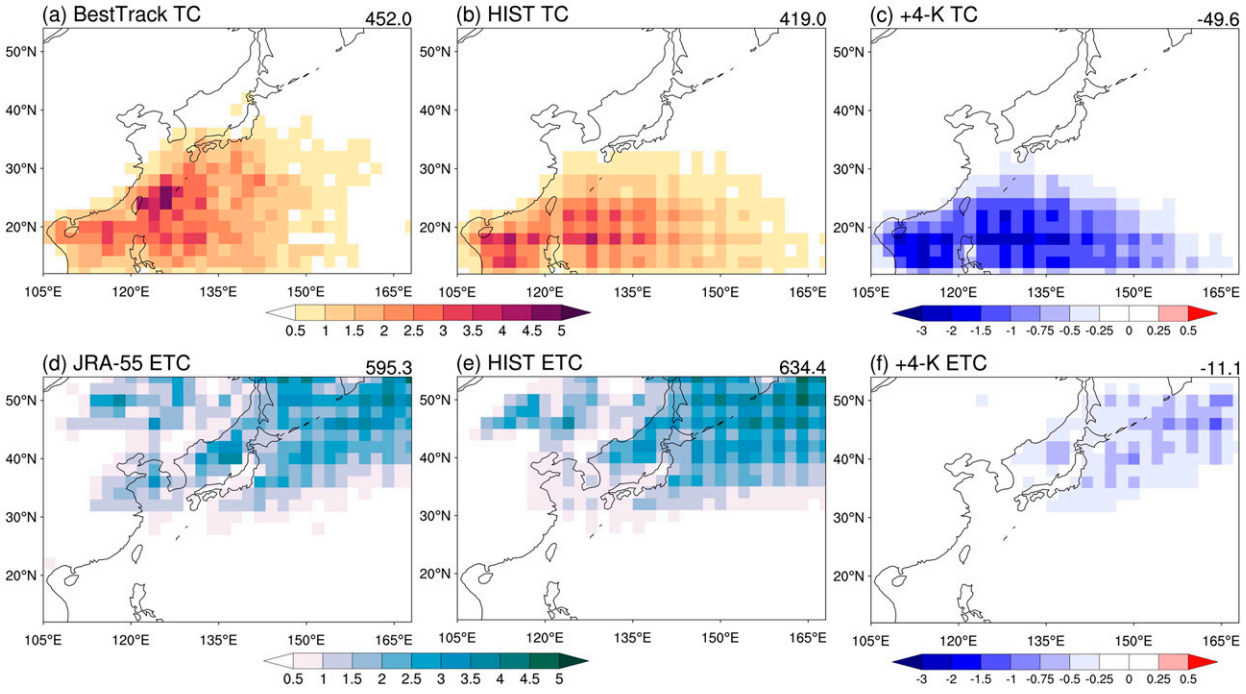


FIG. 2. JASON mean track density from 1979 to 2010 for (a) BestTrack TC, (d) JRA-55 ETC, (b) 50-member MRI-AGCM HIST ensemble TC and (e) 50-member MRI-AGCM HIST ensemble ETC. The number at the top right of the panels represents the annual track density. Also shown are future changes in (c) TC and (f) ETC density between the HIST and +4-K, with percent change of density at the top right of the panels. Tracks are binned at 2° grid intervals.

(Frank and Ritchie 2001). Others have shown that small amounts of shear may be beneficial for TC development (Paterson et al. 2005). Our results may indicate that TCs transition to ETCs prematurely (farther south) when the vertical wind shear criteria for TCs is simply when the maximum wind speed at 850-hPa is greater than the maximum wind speed at 300 hPa.

There are also uncertainties in the BestTrack data, depending on how different agencies estimate TC intensity from satellite data (Kossin and Velden 2004; Kamahori et al. 2006; Barcikowska et al. 2017). In comparing our results with those of Barcikowska et al. (2017), who examined three BestTrack datasets (JMA, China Meteorology Administration, and the Joint Typhoon Warning Center), it is seen that there are similar TC track densities from the JMA but that the latter two exhibit lower track densities near the Ryukyu Islands and are closer in spatial distribution to the results shown in Fig. 2b and in Figs. S1a and S1b in the online supplemental material.

TABLE 1. Annual number of JASON TCs and ETCs from 1979 to 2010 in the WNP (Fig. 2) domain, and those within the black-outlined and red-outlined regions in Fig. 1b for BestTrack, JRA55, ERA5, MRI-AGCM HIST, and +4-K, and for each ΔSST pattern applied for the d4PDF.

| | WNP | | Hokkaido | |
|---|---|---|---|---|
| | TC | ETC | TC | ETC |
| BestTrack | 19.5 | — | 2.7 | — |
| JRA-55 | 18.6 | 54.2 | 2.8 | 22.7 |
| ERA5 | 20.9 | 56.3 | 2.9 | 24.8 |
| HIST | 17.8 | 51.7 | 2.4 | 23.6 |
| +4-K ensemble | 10.3 | 46.1 | 1.9 | 19.0 |
| CCSM4 | 10.7 | 46.3 | 1.6 | 19.5 |
| GFDL-CM3 | 10.6 | 46.7 | 1.9 | 19.0 |
| HadGEM2-AO | 11.4 | 47.2 | 2.2 | 19.7 |
| MIROC5 | 7.0 | 42.7 | 1.7 | 17.2 |
| MPI-ESM-MR | 10.5 | 46.4 | 2.0 | 18.8 |
| MRI-CGCM3 | 11.6 | 47.4 | 2.0 | 19.6 |

For +4-K, a robust decrease of nearly 50% was seen in track density (Fig. 2c), with an ~42% decrease in the number of WNP TCs (Table 1). This decrease is seen in many studies and is identical to the 42% decrease shown by Yoshida et al. (2017), who also used the d4PDF. We note an ~61% decrease for MIROC5 ΔSST (Table 1), while Yoshida et al. (2017) indicated a 74% decrease, both significantly higher than other ΔSST patterns. The lack of heavy precipitation near the Philippines in the MIROC5 was reported by Watanabe et al. (2010), signifying the possibility that tropical disturbances that may later develop into TCs are less frequent than in the other ΔSST patterns.

The annual track density of ETCs from the JRA-55 and MRI-AGCM is shown in Figs. 2d and 2e. The overall spatial distribution of track densities is similar between the two datasets, with ETCs most prominent north of 30°N. Both datasets indicate ETCs over land areas such as eastern China and Mongolia, over the SoJ, and near the Kuroshio–Oyashio

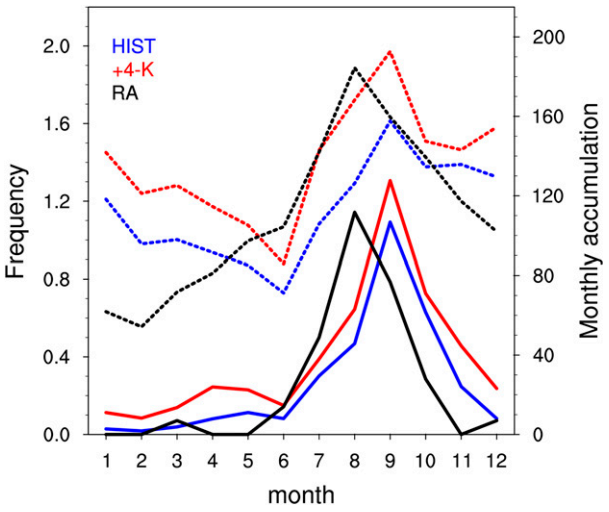


FIG. 3. Monthly mean frequency of WEP (solid lines) and monthly accumulated precipitation (dotted lines; mm) for all grid points in Hokkaido.

Extension (KOE; Fig. 1a) over water, all of which are well-known in East Asia (Adachi and Kimura 2007; Lee et al. 2020). There was a slight overestimation or underestimation in annual ETCs relative to JRA-55 or ERA5 (Fig. S1c in the online supplemental material), respectively, and fewer ETCs are identified in eastern China. Similar to TCs, the ERA5 produces more ETCs than the JRA-55, likely due to finer horizontal grid spacing. For +4-K, there was an ~11% decrease in track density and the number of tracks (Table 1), most of which are north of 35°N (Fig. 2f). These decreases may be attributed to weakened baroclinicity because of a decrease in the future north-to-south temperature gradient (Ito et al. 2016). While the methods may differ, our results are similar to future ETC responses in previous studies (Yettella and Kay 2017; Catto et al. 2019; Sinclair et al. 2020).

### b. *Precipitation characteristics*

We next examined the ability of the NHRCM05 to reproduce general precipitation patterns in comparison with RA. Figure 3 shows the total accumulated precipitation over Hokkaido and the frequency of WEP per month. WEPs are extracted using NHRCM05 HIST thresholds for both climate simulations. The greatest accumulated precipitation and WEP frequency were seen in JASON for RA, HIST, and +4-K, supporting our decision to focus on these months for analysis. HIST exhibits a slight delay in the precipitation peak and an overestimation of winter total precipitation. The delay in HIST precipitation is approximately one to two weeks (not shown). The overestimation in winter total precipitation is likely due to the RA's reliance on surface observations to adjust radar-estimated precipitation. Sparse surface weather stations at higher elevations and the low catch rate of solid particles likely contributed to the underestimation (Yamamoto et al. 2011). The +4-K exhibits more accumulated precipitation throughout the year, with the greatest differences seen in July–September, likely attributable to the increase in WEP frequency.

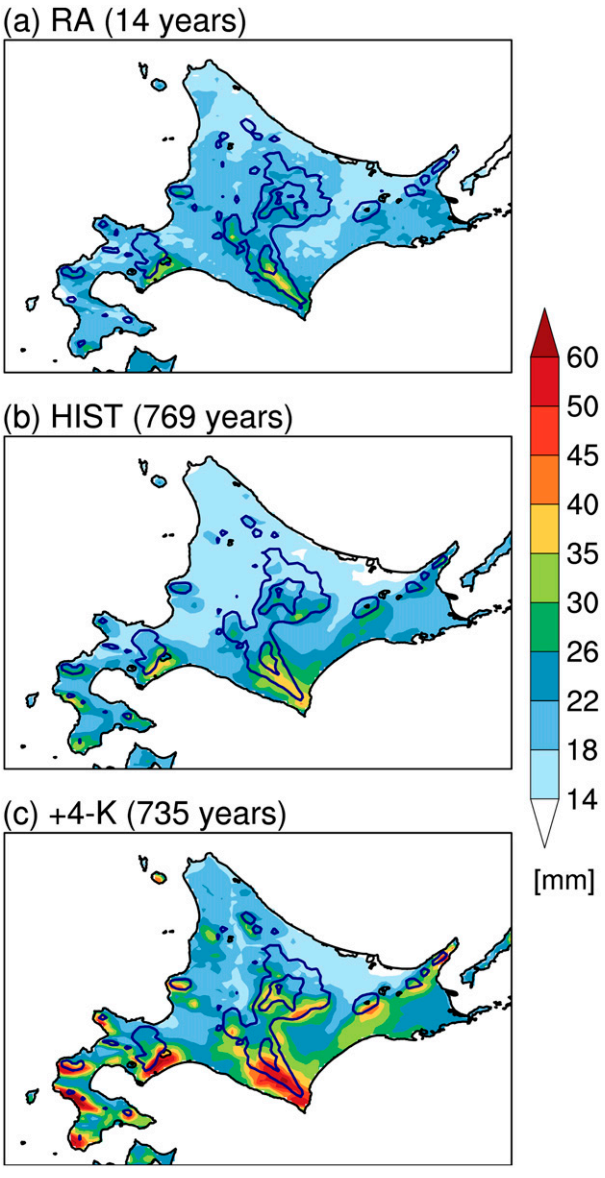


FIG. 4. Spatial distribution of 99th-percentile JASON precipitation (mm) for (a) RA, (b) HIST NHRCM05, and (c) +4-K NHRCM05. The blue contours represent orography at 500-m intervals. For RA orography, the 2-minute gridded global relief data (ETOPO2v2; NOAA/National Geophysical Data Center 2006) were used and regridded to the same 5-km grid as the NHRCM05.

The 99th-percentile JASON precipitation was examined for spatial reproducibility (Fig. 4). The HIST provides a much smoother rendition than RA due to its robust sample size, but the geographical patterns are similar. High precipitation amounts near southern Hokkaido, such as near the Hidaka mountains and the southern side of higher elevations farther west, are present in both datasets. There is a slight overestimation in the Oshima Peninsula and an

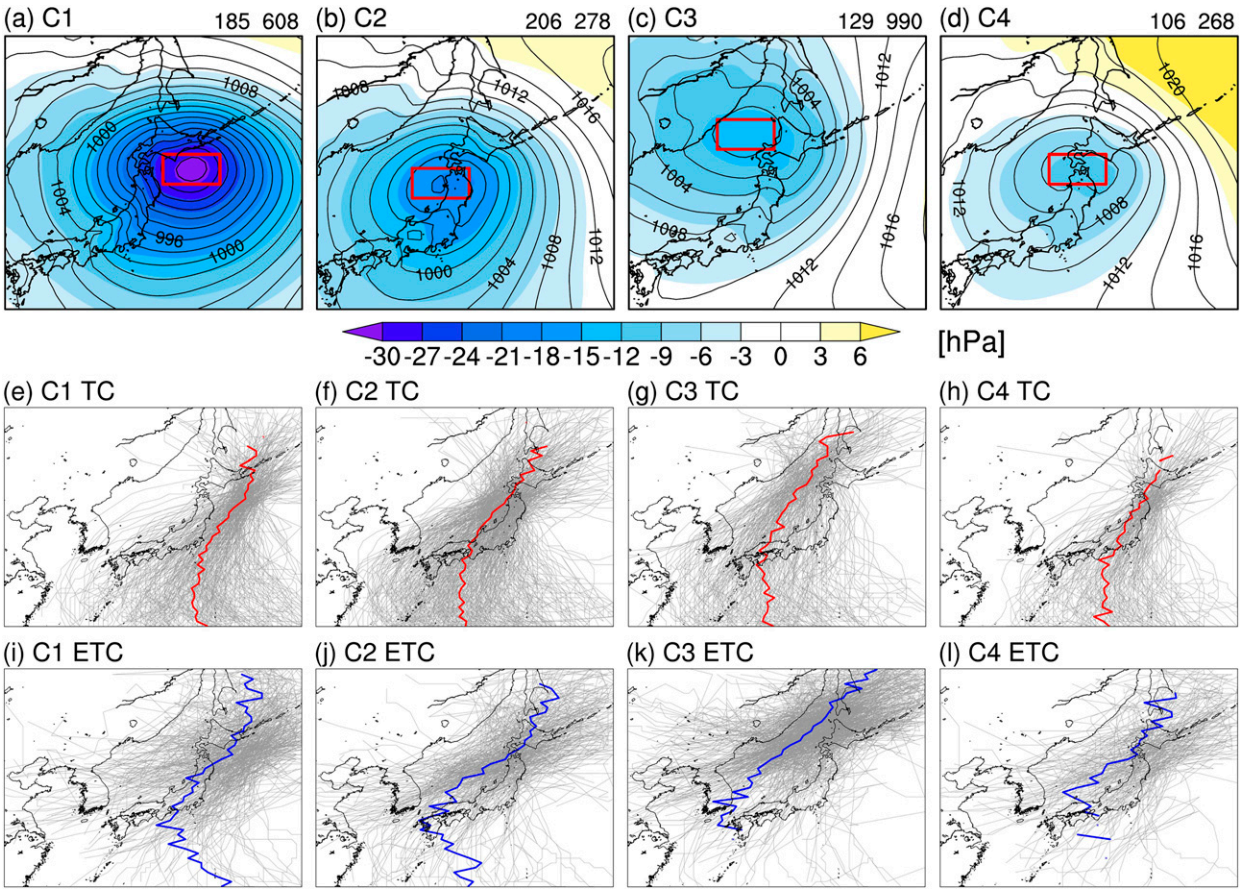


FIG. 5. (a)–(d) Four cyclone patterns resulting in WEPs determined using *K*-means clustering. SLP is contoured (2-hPa interval), and SLP anomalies (computed from a 60-yr daily climatology for each ensemble) are shaded. The red-outlined box indicates the domain used to extract cyclones in similar weather patterns. The numbers at the top right of each panel represent TC and ETC frequency, respectively, for each cluster. Also shown are the tracks for (e)–(h) TCs and (i)–(l) ETCs in each cluster. Individual tracks (6 hourly) are in gray, and the latitudinal averages are in red (TC) and blue (ETC). Averages are plotted for each latitude with 20 or more tracks.

underestimation in central Hokkaido, though both can be attributed to fewer years in RA than HIST. For +4-K, there are large precipitation increases, particularly in the southern half of Hokkaido. On the southern flanks of the mountains, moist flow from the south and orographic ascent contribute to enhanced precipitation there (Inatsu et al. 2015). In addition to the increase in WEP, the duration of WEPs is projected to increase in +4-K (Table S1 in the online supplemental material). While increased water capacity resulting from a warming climate may contribute to these results, it is likely that many of these widespread events are cyclone induced, meaning that additional factors such as TC/ETC intensity, translation speed, or size may have also contributed (discussed in section 4). Regardless of the mechanisms, longer, more frequent, and more intense WEPs appear likely in a warmer climate.

Results from the *K*-means clustering on WEP are shown in Figs. 5a–d, comprising 626 TC and 2144 ETC events. We make no distinction between TC or ETC origin or trajectory/path traveled for our study. Three of the four patterns are distinct from each other. C1 depicts a deep cyclone southeast of Hokkaido; in C2, the cyclone center is just northwest of Honshu, and in C3, the cyclone center is over the northern Sea of Japan. C4 is similar to C2 but with a much weaker (~10 hPa) cyclone center. C1 and C3 contribute to a majority of ETCs between the four clusters, while C2 contributes roughly a third of all TCs between the four clusters. Increasing the number of clusters does not produce additional distinguishable SLP patterns.

Individual cyclone tracks for each cluster (defined as all cyclone tracks that pass within 2° from each cluster's SLP minimum) are shown in Figs. 5e–l. For TCs, the majority of tracks originate from the tropical WNP, as expected. C1 includes many of the strongest TCs (lowest SLP minima) owing to less rapid weakening from less land interaction. C2 and C3 TC tracks are quite similar, with some tracks traversing the Japanese islands before entering the SoJ and others entering the region from near the Korean Peninsula. The weak intensity of TCs in C4 (Fig. 5d) is likely due to the prolonged land interaction. ETC tracks are quite different from those of TCs, with more tracks farther west and north. While several tracks

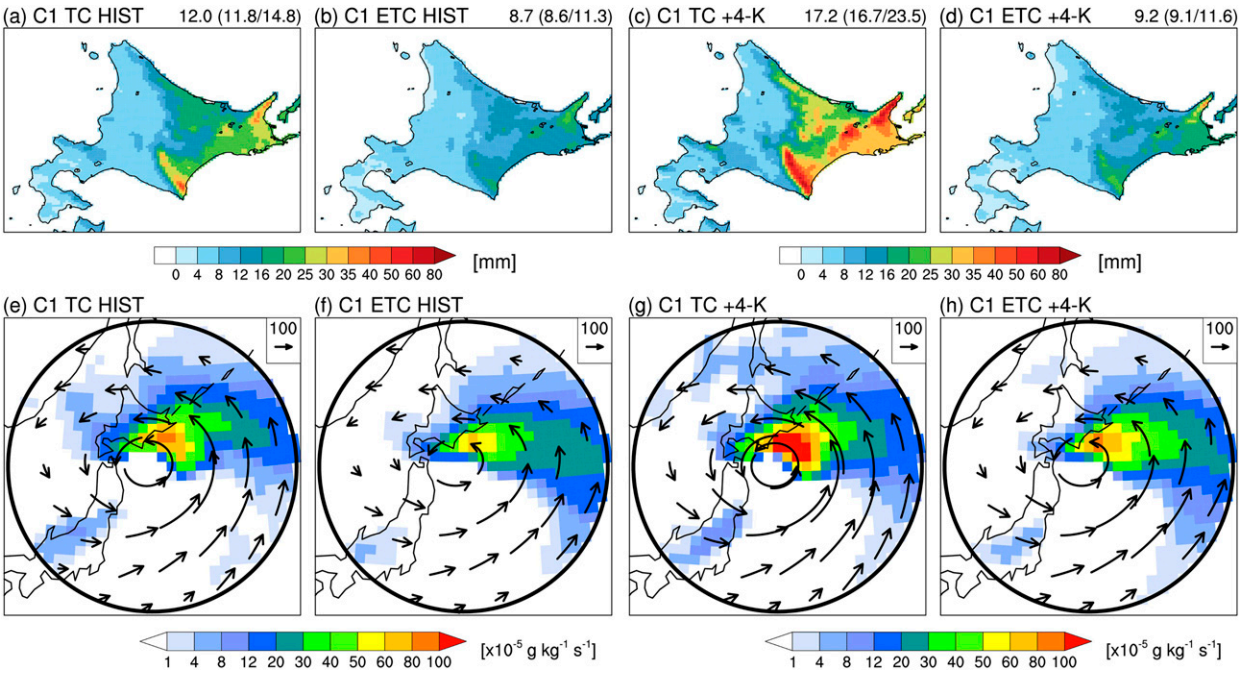


FIG. 6. Composite (top) precipitation and (bottom) MF850 (vectors; g kg$^{-1}$ m s$^{-1}$) and MFC850 (shading; $10^{-5}$ g kg$^{-1}$ s$^{-1}$) for TC- or ETC-associated (as labeled) precipitation for C1 for (a),(b),(e),(f) HIST and (c),(d),(g),(h) +4-K. The number at the top right in (a)–(d) represents precipitation averaged over all grid points in Hokkaido, precipitation amounts for grids below 250 m and above 750 m shown in parentheses. The bottom panels are 8° radial composites centered at TC and ETC SLP minima. MF850 vectors less than 80 g kg$^{-1}$ m s$^{-1}$ are omitted for clarity.

are likely transitioned TCs, many originate over the Asian continent, and there is greater track density over the SoJ. C1 also exhibits greater ETC track density over the KOE region southeast of Hokkaido, meaning that these ETCs are likely to be more intense due to stronger low-level baroclinicity (greater meridional SST gradient) than in other clusters. C2 and C3 are similar, with high track densities over the SoJ likely signifying intensifying ETCs moving northeastward into a region of strong SST gradient, with C3 displaced farther north. Some of these ETCs are likely remnants of TCs that transition before approaching Hokkaido. C4 is similar to C2, suggesting that many of the ETCs in C4 resided near the C2 location earlier.

### c. *Future changes in precipitation and moisture flux characteristics*

Next, we focused on the geographic distribution of precipitation by separating TCs and ETCs for each cluster and investigating how they are projected to change in +4-K. We focus on events with SLP minima <990-hPa for all time steps in the NHRCM05, which is equivalent to category 1 hurricane intensity introduced by Klotzbach et al. (2020) and categorized as "relatively deep cyclones" in Catto et al. (2019).

For C1, TCs produce a larger area of heavy precipitation than ETCs, regardless of elevation (Figs. 6a–d). MF850 for both TCs and ETCs exhibit south-southeasterly flow in the northeast quadrant near the cyclone center, and the greatest MFC850 corresponds to the location of the heaviest precipitation in the eastern half of Hokkaido (Figs. 6e–h). TCs exhibit stronger MF850 and MFC850 than ETCs, contributing to more precipitation for TCs. For +4-K, there is higher precipitation in TCs and very little change in ETCs. There is an ~43% increase in area-averaged precipitation for TCs and greater increases at higher elevations (~59%). ETCs exhibit only an ~6% increase in area-averaged precipitation. This difference can be attributed to the larger increases in MF850 and MFC850 for TCs, likely due to a larger projected increase in TC intensity than ETC intensity (discussed in section 4a).

Cluster C2 exhibits precipitation predominantly in southern Hokkaido, with highest intensities east of the Hidaka Mountain range and over Oshima Peninsula and higher-elevation areas in southern Hokkaido. TCs exhibit greater precipitation than ETCs, but less precipitation than C1 because the cyclone center is farther from Hokkaido (Figs. 7a,b). Differences in precipitation may again be attributed to MF850 and MFC850 (Figs. 7e–h), as large values extend farther northeast for TCs, affecting larger portions of Hokkaido than for ETCs, for which MF850 is weaker and high MFC850 is confined closer to the center of ETCs. For +4-K, there is a ~25% increase in TC precipitation, but with little difference based on elevation because much of the Oshima Peninsula (Fig. 1a) is at relatively low elevations, where much of the precipitation changes are projected. ETCs exhibit very little change in precipitation. MF850 and MFC850 are greater for TCs, again contributing to increased precipitation. ETCs also exhibit enhanced MF850 and MFC850 but are again concentrated near the ETC center, limiting the impact on Hokkaido.

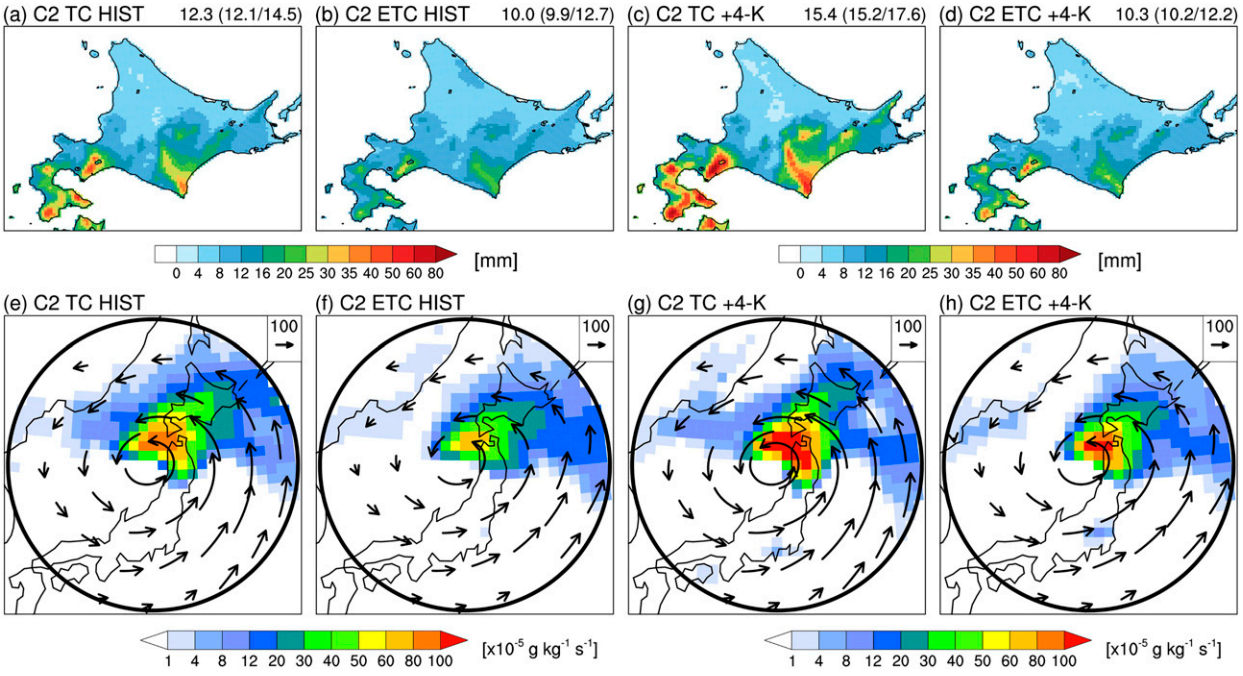


FIG. 7. As in Fig. 6, but for C2.

Cluster C3 produces the lowest precipitation for both TCs and ETCs between the four clusters and is concentrated at high elevations (Figs. 8a–d). Unlike the other clusters, Hokkaido is in the southeastern quadrant of the cyclones (Fig. 5c), removing it from the cyclone-induced MFC850, which is greatest in the northern half and near the center of cyclones. Therefore, this cyclone placement produces westerly to southwesterly MF850 in southern Hokkaido. The patterns for +4-K are very similar. There is a 32% increase in precipitation for TCs and a 30% increase for ETCs, and only marginal differences based on elevation for TCs (39% at higher elevations and 32% at lower elevations) and ETCs (22%–31%). This is perhaps because of

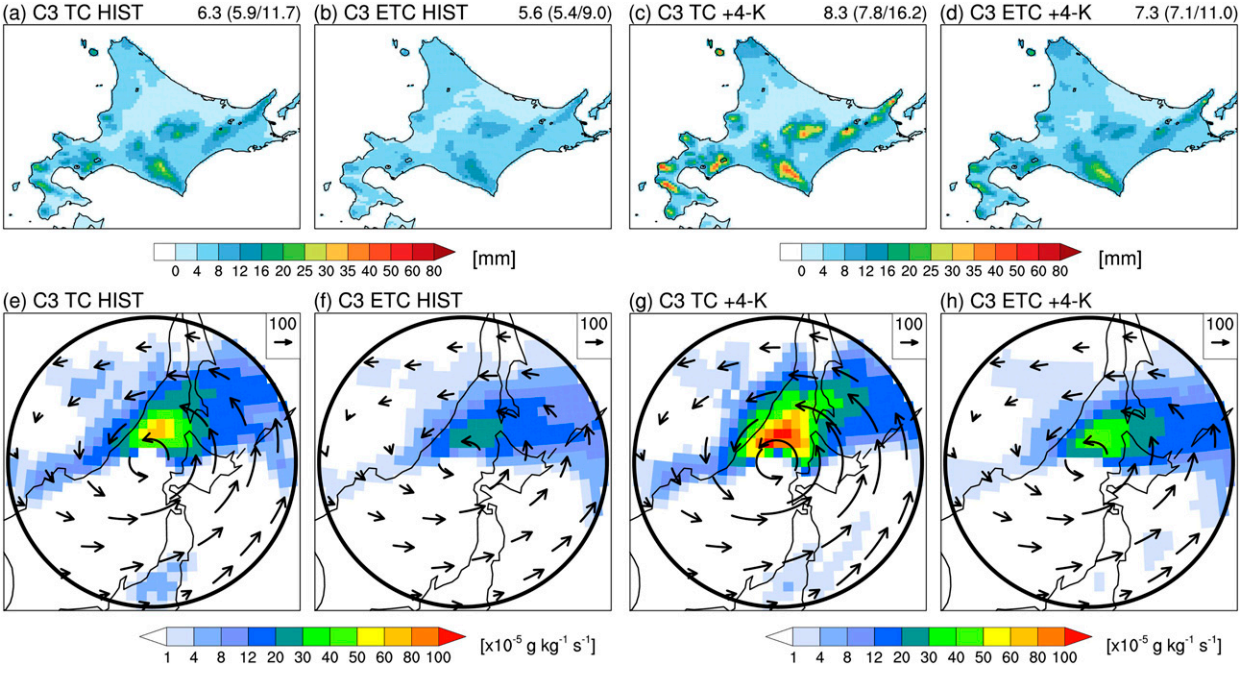


FIG. 8. As in Fig. 6, but for C3.

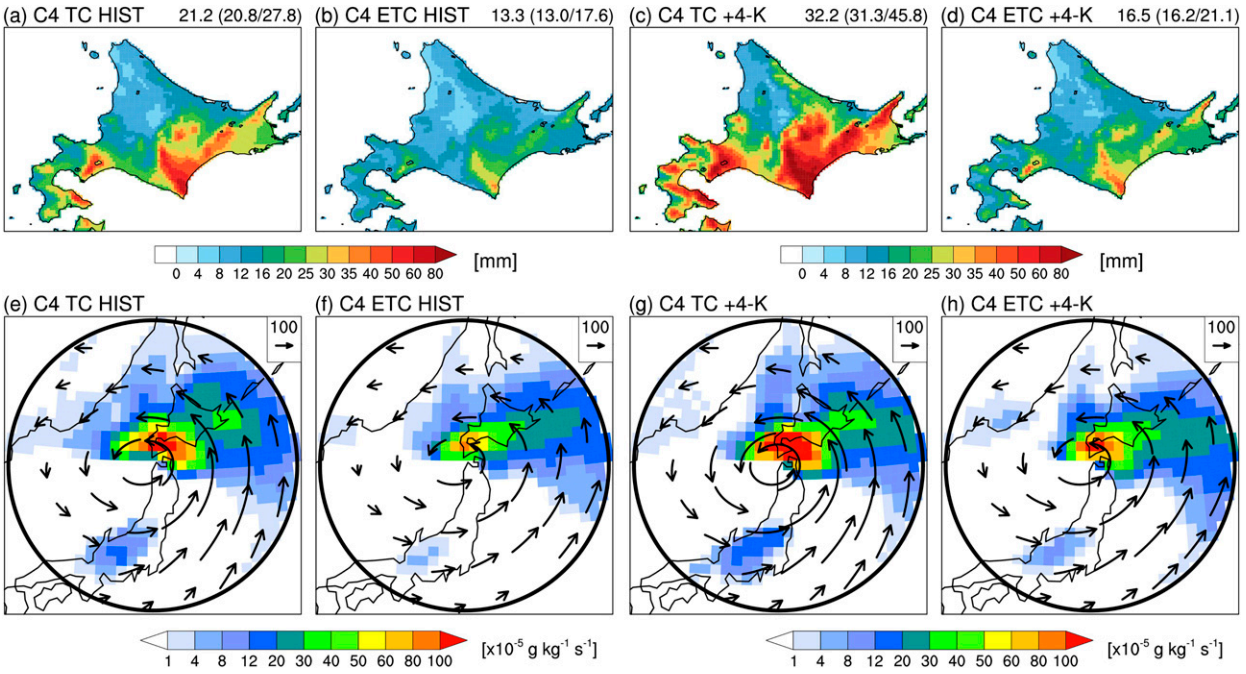


FIG. 9. As in Fig. 6, but for C4.

the lack of change in MFC850, and the MF850 change is similar between TCs and ETCs. There is also a slight increase in precipitation over northern Hokkaido for TCs and ETCs, where a slight increase in MF850 and MFC850 east of the cyclone center may have contributed to increased precipitation.

Last, C4 exhibits large areas in southern Hokkaido with high precipitation amounts (Figs. 9a–d), regardless of cyclone type, because much of Hokkaido is close to the strongest MF850 and MFC850 (Figs. 9e–h). TCs again produce heavier precipitation than ETCs because TCs exhibit stronger MF850 and MFC850 than ETCs and over a larger area. The difference in precipitation amounts between TCs and ETCs was again attributed to the difference in MF850 and MFC850, as TCs show stronger features for both than ETCs, and for a larger area. MF850 and MFC850 for TCs are projected to increase significantly, resulting in a 52% increase in TC-associated precipitation, with greater future change at higher elevations than lower elevations (65%–50%). ETCs exhibit a 24% increase (similar at high and low elevations) owing to smaller increases in MF850 and MFC850, particularly in the right-front quadrant of the cyclones.

## 4. Discussion

TCs and ETCs are projected to produce heavier precipitation in Hokkaido in a warmer climate, with the largest projected increases owing to TCs. We now discuss how cyclone intensity, speed, and size may change, all of which can influence the frequency, intensity, and duration of future WEPs.

### *a. Intensity*

SLP minima for all cyclones approaching Hokkaido are shown in Fig. 10. As expected, there are more TCs with lower SLP than ETCs in both the JRA-55 and HIST datasets. TCs (Figs. 10a,b) are stronger in the SoJ and PO in future climates, particularly the strongest storms. ETC (Figs. 10c,d) intensities are largely consistent between HIST and +4-K. For both types of cyclones and domains, PO cyclones are deeper than those in the SoJ because TCs often interact with land before entering the SoJ, and ETCs are usually early in their life cycle or experience less low-level baroclinic instability relative to the PO (Adachi and Kimura 2007; Lee et al. 2020).

TCs develop in regions of warm SSTs and weak vertical wind shear. As SSTs are projected to increase (Fig. S2 in the online supplemental material) and vertical wind shear is projected to decrease (Fig. 11) over much of the area around Japan from July to November, future climate projections indicate environmental conditions that favor TC development or extratropical transition farther north than in the current climate, consistent with previous studies (Yasuda et al. 2010; Murakami et al. 2012). There is also a greater fraction of WNP TCs approaching Hokkaido in +4-K (~18%) than in HIST (~13%). The more intense +4-K TCs, as well as stronger MF850 and MFC850 (Figs. 6–9), likely contributed significantly to the heavier TC-induced precipitation in +4-K.

For all ΔSST patterns used for +4-K ensemble experiments, the CCSM4 exhibits the smallest change in TC intensity, while the GFDL-CM3 shows the greatest intensification in both basins (Table S2 in the online supplemental material). The CCSM4 SST patterns also show the least warming south of ~45°N, while the GFDL-CM3 exhibits some of the most intense warming, favoring TCs maintaining their intensity as the move toward Hokkaido. The MIROC5 also showed an intensification of TCs in the PO region, which coincides with SST warming similar to the GFDL-CM3 and strong decreases

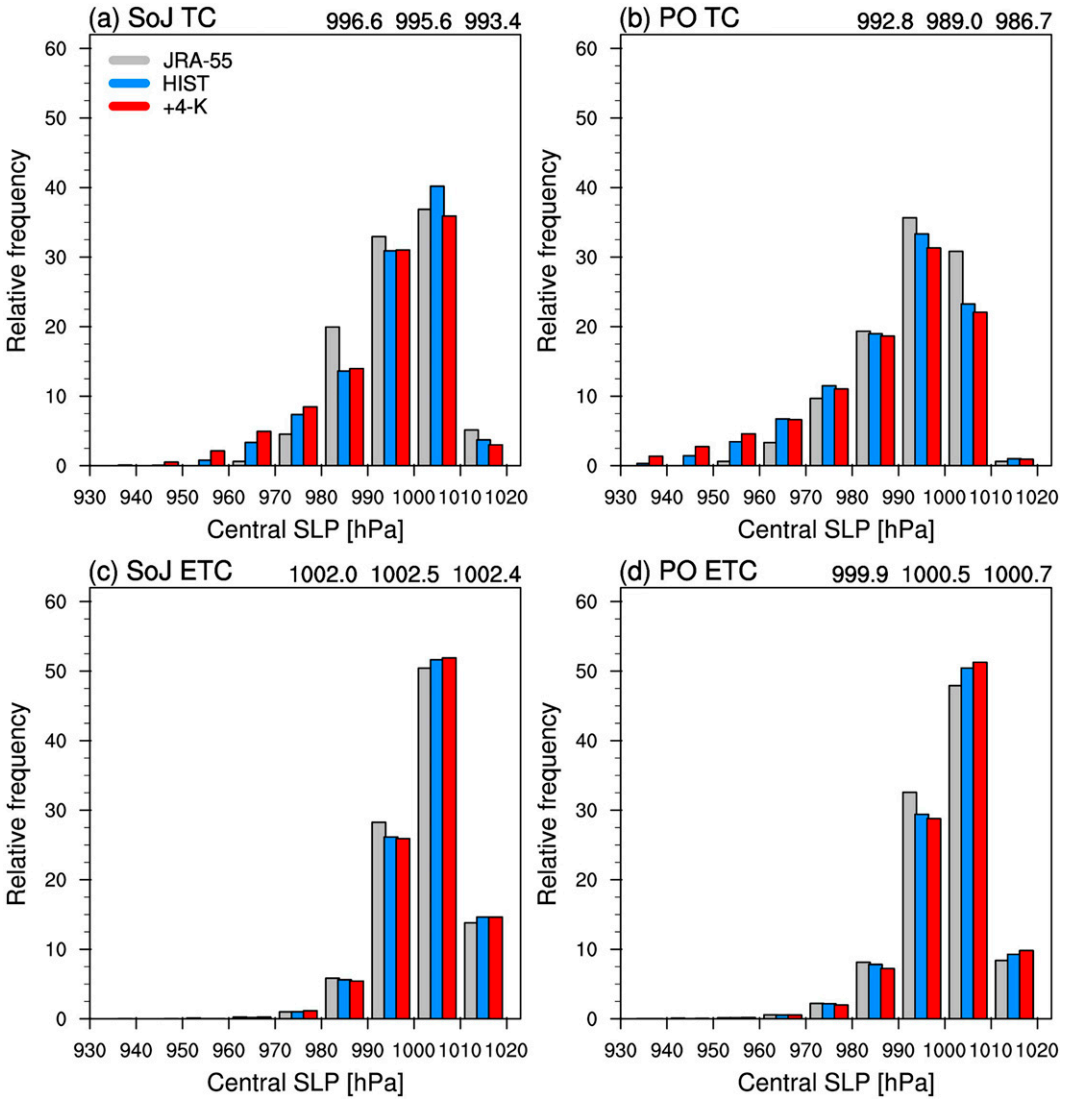


FIG. 10. Minimum SLP (hPa) of all (a),(b) TCs and (c),(d) ETCs in the proximity of Hokkaido, separated by ocean basins. The numbers at the top right of each panel indicate the average SLP from JRA-55, HIST, and +4-K, respectively.

in vertical shear (Fig. S3 in the online supplemental material) during peak TC months. Interestingly, models such as the CCSM4 exhibit decreased mean intensity in the PO domain, despite warming SSTs and decreasing vertical shear, which is also seen for SoJ TCs in the MIROC5, highlighting the uncertainties of how future environmental changes may ultimately impact the intensity of TCs.

The lack of ETC intensity change is consistent with previous studies (Hawcroft et al. 2018; Catto et al. 2019), and precipitation changes are more likely to be driven by increased moisture than by changing dynamics, which is seen in the MF850 and MFC850 analyses. ETC intensity based on ΔSST patterns showed some variability, particularly in the SoJ region, but is consistent with the overall +4-K ensemble change.

### b. *Translation speed*

Figures 12a and 12b show the translation speed of TCs. In HIST, PO TCs traveled slightly faster than those in the SoJ. Translation speeds are heavily influenced by upper-level flow, and the PO exhibits a slightly stronger 500-hPa flow than the SoJ (Fig. 13), resulting in faster-moving PO-based TCs. The overall distribution and interarea differences between JRA-55 and HIST are consistent, albeit with slightly faster translation speed for the reanalysis. However, the sample size for the JRA-55 may not be sufficient for comparison, particularly in the SoJ, where only 46 time steps are examined. This may partly explain why TCs exhibit faster movement in the SoJ than in the PO for the JRA-55 as compared with the HIST ensemble. There is a decrease in translational speed for

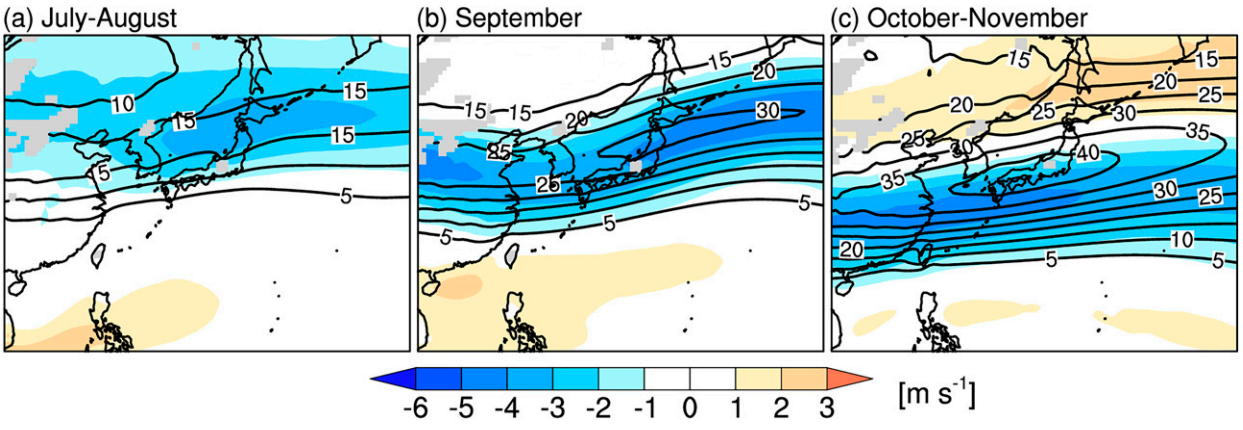


FIG. 11. Climatological 300–850-hPa vertical wind shear (m $s^{-1}$) for (a) July–August, (b) September, and (c) October–November. Contours represent HIST climate, and shading represents +4-K change (+4-K − HIST).

all ocean-based storms in +4-K climate, as TCs slow by ~6% and ~8% for the SoJ and PO basins, respectively. Both the SoJ and PO domains exhibit slower 500-hPa flow in +4-K, with a greater decrease over the PO domain. However, there is quite a bit of variability in translation speed between the ΔSST patterns (Table S4 in the online supplemental material), which can be directly attributed to variability in 500-hPa winds. During peak TC months, the MIROC5 shows the greatest decrease in 500-hPa winds near Japan (Fig. 14), yielding the slowest translation speeds of all ΔSST patterns. The HadGEM2-AO also exhibits a marked slowdown in TCs, which can also be linked to relatively large decreases in 500-hPa winds. Conversely, the GFDL-CM3 and MRI-CGCM3 depict a slight acceleration in translation speed despite a decrease in 500-hPa winds. Thus, the slower TCs in the +4-K ensemble are not only owing to changes in the 500-hPa winds, consistent with Yamaguchi and Maeda (2020), who also utilized the d4PDF dataset but for a much larger analysis domain.

Another large-scale feature that influences TC speeds is the WNPSH (Wang et al. 2020). To examine potential changes to the extent and intensity of the WNPSH, we used the eddy geopotential height (He; Zhou et al. 2009; He et al. 2015), which is the departure of 500-hPa geopotential height (gpm) relative to the zonal mean between 0° and 40°N (Fig. 14). Using the 0-gpm He as WNPSH extent and 10-gpm He to approximate its strength, all ΔSST patterns exhibit minimal change or an eastward repositioning of the WNPSH. The eastward retreat or weakening of the WNPSH has been reported in previous studies (Murakami et al. 2011; Ose et al. 2020; Takabatake and Inatsu 2022), though there are uncertainties in these projected changes (He and Zhou 2015). The CCSM and GFDL-CM3 show minimal change in the WNPSH, while the HadGEM2-AO and the MIROC5 exhibit a strong eastward retreat. The ΔSST patterns exhibiting minimal changes in the WNPSH also tend to show little change in translation speeds of TCs, while those with a robust weakening of the WNPSH show the greatest deceleration.

ETC translation speeds, which are rarely examined relative to TC translation speeds, are shown in Figs. 12c and 12d. For ETCs, there appears to be a slight acceleration in all basins, which runs contrary to the decreased midlevel flow. However, while TCs are most prominent between July and September in the WNP due to their dependence on warm SSTs, there is less seasonality for ETCs (Table S3 in the online supplemental material). ETCs can develop year-round through multiple processes such as lee cyclogenesis over the Asian continent, sharp SST gradients near the KOE, or through TC to ETC transitions. Upon closer examination, ETCs south of 43.5°N slow by ~6% over the SoJ and PO basins, and north of there they exhibit a speed increase by 20% in the SoJ and 7% in PO.[1] In October–November, as 500-hPa winds are projected to increase north of Hokkaido in +4-K, ETCs are projected to accelerate, though farther south, where 500-hPa winds are projected to decrease, translation speed also decreases. The acceleration in northern latitudes in October–November may coincide with a potential northward displacement of the subtropical jet due to a warming climate (Hirahara et al. 2012). Different ΔSST patterns are very similar, with the HadGEM2-AO being the lone model with slightly decreasing translation speeds throughout both PO and SoJ domains. This model exhibits a slowdown in 500-hPa winds across the entire analysis domain (Fig. 1b) in October–November (Fig. S4 in the online supplemental material), slowing ETC speeds. Other patterns indicate either little change (CCSM4) or a dipole pattern of increasing and decreasing 500-hPa flow similar to the +4-K ensemble results, leading to little change in translation speeds.

### c. *Size*

For TCs (Figs. 15a,b), both SoJ and PO basins exhibit a decrease in size (10% and 4%, respectively) in +4-K, with similar decreases seen between ΔSST patterns (Table S5 in the online supplemental material). The potential shrinkage of TCs in the WNP was also reported using high-resolution AGCMs driven by CMIP5 SSTs (Knutson et al. 2015) and for TCs approaching Hokkaido in 4-km grid spaced pseudo–global

[1] The number of ETCs compared is nearly identical between the HIST (16.9 $yr^{-1}$ northern ETCs vs 17.4 $yr^{-1}$ southern ETCs) and +4 K (13.9 vs 13.6 $yr^{-1}$) ensembles.

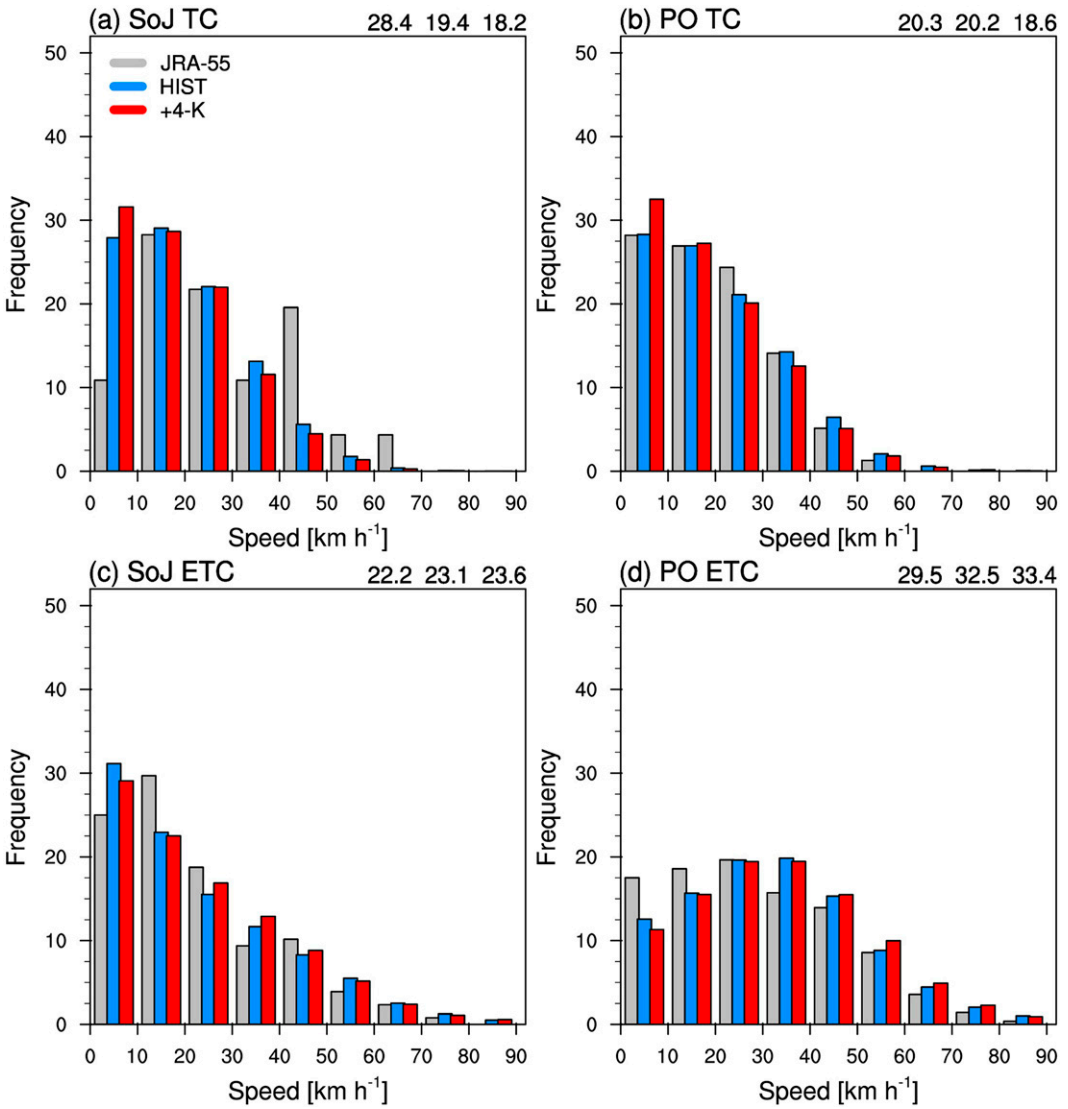


FIG. 12. As in Fig. 10, but for translational speed (km $h^{-1}$) for cyclones with SLP minima of <990 hPa.

warming experiments utilizing d4PDF (Kanada et al. 2020). Using four 5-km grid spaced nonhydrostatic models, Kanada et al. (2017b) suggested through pseudo–global warming experiments that a warmer climate leads to increased water vapor in the lower troposphere, resulting in a contracted radius of maximum winds due to stronger eyewall convection. Although they only simulated one typhoon (Typhoon Vera), it was suggested that other intense TCs would likely respond similarly to a warming climate. However, contrasting responses of TC size to global warming are also reported in several studies (Kim et al. 2014; Sun et al. 2017; Yamada et al. 2017). Both Sun et al. (2017) and Yamada et al. (2017) attribute the increase in projected TC size to increased instability and stronger convection in the outer regions of the storm, which may be more important in dictating TC size than inner core dynamics (Chan and Chan 2015). However, Wu et al. (2015) suggest that a horizontal grid spacing of less than 10 km may be required to investigate the mechanisms governing TC sizes. Further research is therefore needed to provide better reasoning for our results.

The smaller ETCs in the SoJ (Fig. 15c) are likely due to the combined factors of a weaker SST gradient relative to the PO (Fig. 15d) and because many initially continental ETCs are in their early development stage over the SoJ. The latter reason was identified by Simmonds (2000), who found that Northern Hemisphere ETCs continued to expand up to around five days after cyclogenesis. For PO ETCs (Fig. 15d), both HIST and +4-K indicate larger sizes than TCs, partly due to many Asian-continent and KOE genesis cyclones propagating into regions with high SST gradients and strong low-level baroclinicity (Yoshida and Asuma 2004). Lee et al. (2020) showed that the maximum Eady growth rate, an indicator of baroclinic instability, is

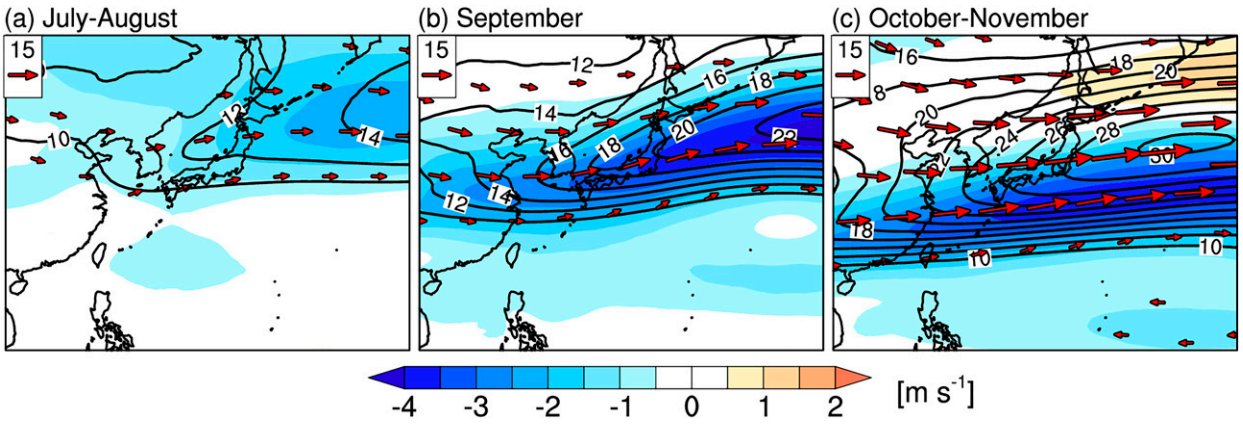


FIG. 13. Climatological 500-hPa flow (m $s^{-1}$) for (a) July–August, (b) September, and (c) October–November. Contours represent HIST, shading represents +4-K change (+4-K − HIST), and vectors represent 500-hPa winds for HIST.

greatest east of Japan, where the meridional SST gradient is highest in the WNP. A weaker projected SST gradient due to more poleward warming may have contributed to a slower ETC growth in +4-K, thus resulting in smaller ETCs in future climates. This is somewhat implied in the ΔSST patterns (Table S5 in the online supplemental material). For example, the GFDL-CM3 and HadGEM2-AO project the greatest warming of SSTs surrounding Hokkaido and northward toward the Okhotsk Sea, corresponding to smaller ETCs in the PO than the other patterns. Conversely, the MPI-ESM-MR and MRI-CGCM3 exhibit a lower increase in SSTs, which may have contributed to less size shrinkage. We note, however, that while MIROC5 also exhibits SST warming similar to the HadGEM2-AO, the ETC size is more comparable to MPI-ESM-MR and MRI-CGCM3. Further studies are therefore needed to understand the mechanisms contributing to future changes in ETC size.

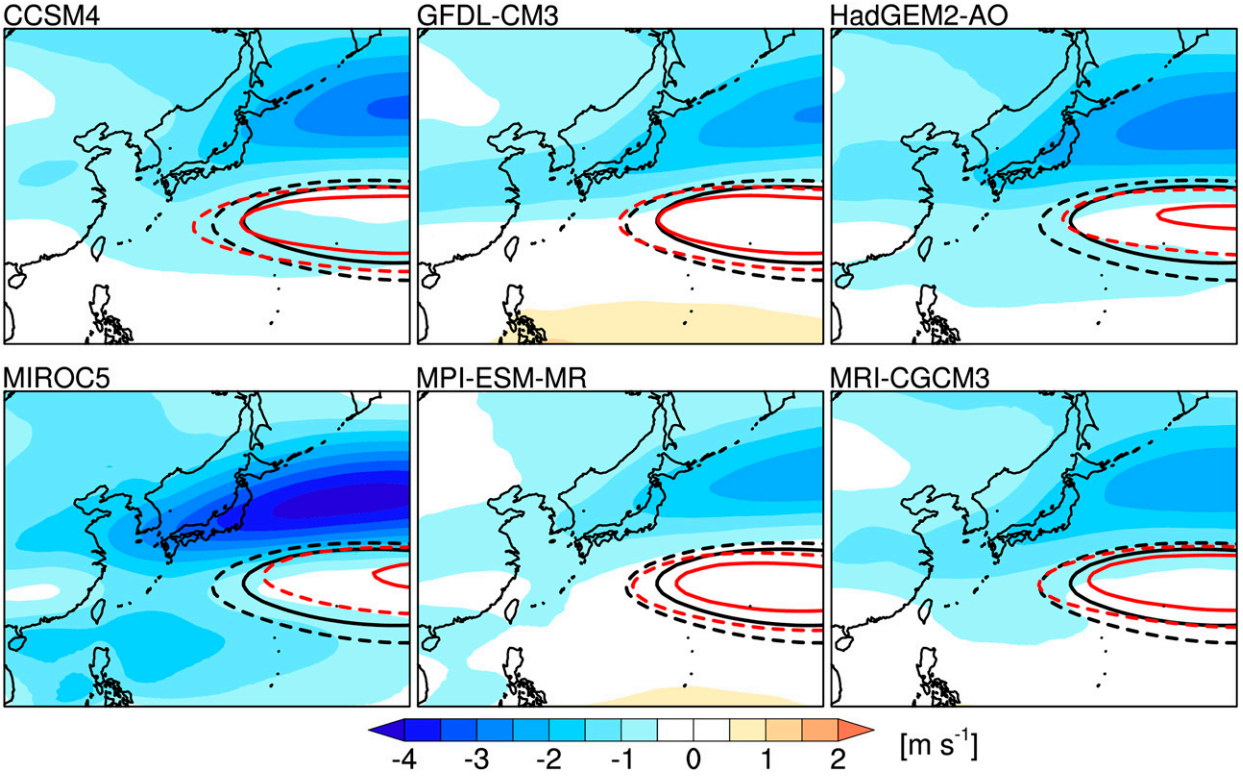


FIG. 14. Climatological change (+4-K − HIST) in 500-hPa flow (shaded; m $s^{-1}$) for July–September. Lines indicate the extent (dotted; 0-gpm He) and strength (solid; 10-gpm He) of the WNPSH. Black lines represent HIST, and red lines represent +4-K.

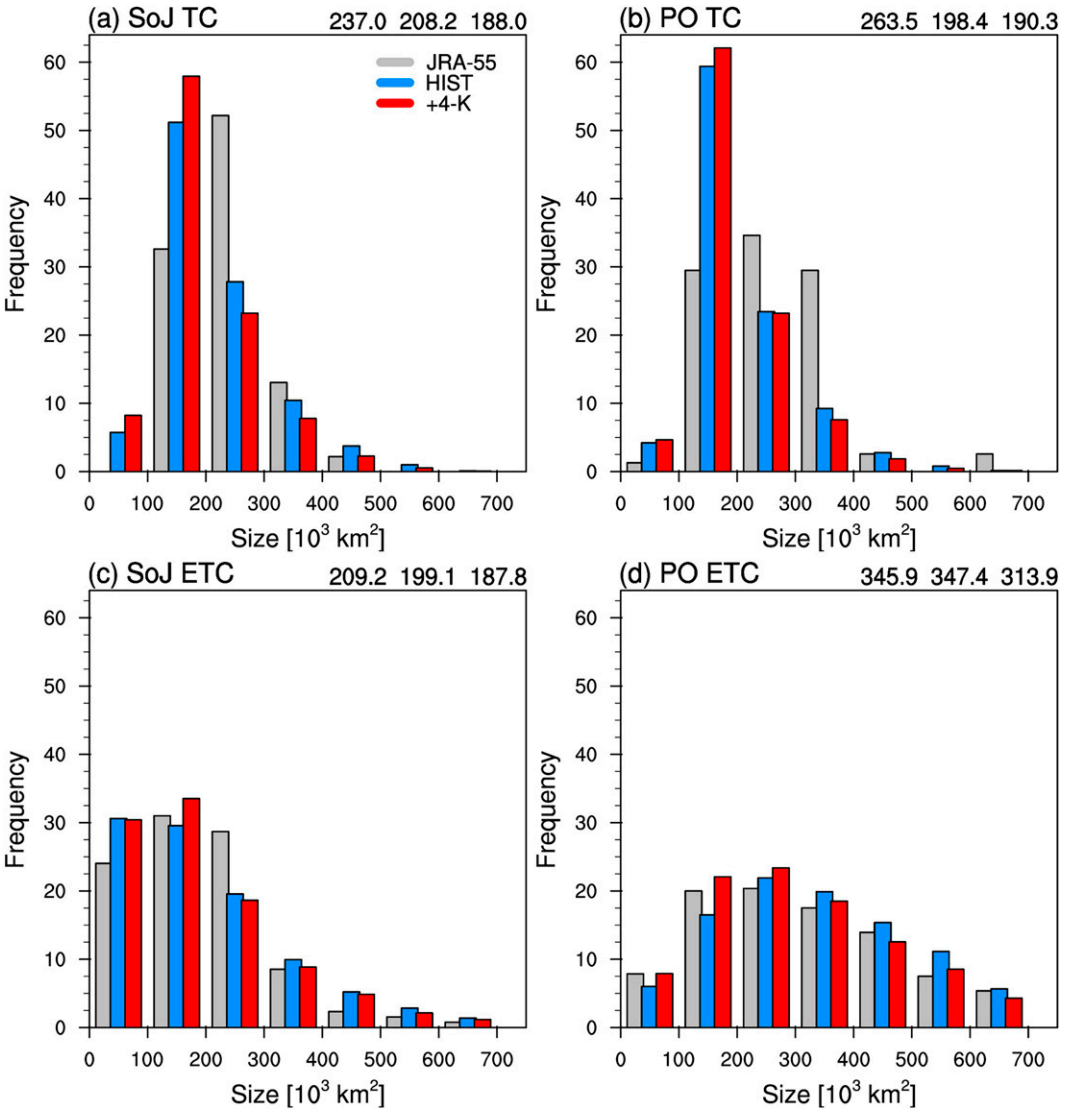


FIG. 15. As in Fig. 10, but for the size of cyclones ($10^3$ km$^2$) with SLP minima of <990-hPa.

## 5. Summary

This study examines the effects of a warming climate on WEPs in Hokkaido using the d4PDF large ensemble dataset. More specifically, we focus on the direct impacts of TC and ETC-associated precipitation, which have been examined extensively in previous studies, but often not simultaneously and at regional levels. We aim to provide a more comprehensive perspective into how and why precipitation may change in response to the 4-K warming climate and how such changes may differ for TCs and ETCs. In addition to examining WEPs, we also examined projected changes in cyclone intensity, translation speed, and size, all of which can affect how impactful a particular event may become.

Using the NEAT tracking algorithm on the MRI-AGCM large ensemble, robust decreases were seen in TC frequency in +4-K for the WNP (~42%) and particularly for TCs over southeast Asia. Only slight decreases were seen in ETCs (~11%), mainly north of 35°N over Japan. Despite the decline in TCs and ETCs, precipitation characteristics such as WEP duration and intensity exhibit an increase in +4-K simulations. This was partly attributed to projected increases in MF850 and MFC850. Both TCs and ETCs show marked increases in MF850 for cyclones with similar positioning, while TCs exhibit greater MF850 and MFC850, contributing to greater increases in precipitation for TCs than ETCs. While TCs yield more extreme precipitation events than ETCs in future climate scenarios, ETCs are much more prevalent and occur year-round, highlighting the importance of examining both types of cyclonic systems to understand how precipitation may change in future climates.

Intense TCs approaching Hokkaido are more frequent in +4-K, while ETCs exhibit minimal changes in intensity, consistent with previous studies. The TC intensity change was

attributed to both warmer projected SSTs and decreased vertical wind shear in +4-K, resulting in TCs maintaining their strength at higher latitudes. Mean TC translation speeds decreased in +4-K by roughly 7% in the SoJ and PO basins, which is related to weakened 500-hPa flow, though variability exists in the magnitude of the slowdown, or lack thereof, based on d4PDF ΔSST patterns. ETCs, on the other hand, exhibit a minimal change in speed (~2% in both basins), partly due to ETCs exhibiting a slowdown south of Hokkaido and acceleration north of Hokkaido, coinciding with areas of decreasing and increasing 500-hPa flow in +4-K. Last, cyclone size for both TCs (~10% in SoJ and ~4% in PO) and ETCs (~6% and ~10%) will likely become smaller.

At 60-km horizontal grid spacing, there are limitations to what can truly be resolved, especially for TCs. In addition, the lack of atmosphere–ocean coupling omits cold wakes under TCs, leading to an overestimation of TCs in the MRI-AGCM (Hasegawa and Emori 2007; Ogata et al. 2016). However, continued improvements to even relatively coarse models have substantially increased model reliability to reproduce TCs and ETCs in recent years (e.g., Catto et al. 2010; Murakami et al. 2012), and AGCMs alleviate the massive computational demand required for coupled models, allowing for more ensemble simulations and greater sample size to examine low-frequency events more thoroughly, a significant advantage of the d4PDF. As we were able to evaluate 700+ yr of TC and ETC-associated WEP, further confidence can be gained from our results, which will hopefully provide some additional insight into how the climate of Hokkaido will change as it continues warming.

*Acknowledgments.* We are very grateful to Editor Dr. Qi Hu and three anonymous reviewers for their constructive comments, which greatly improved the paper. This work is supported by the Environment Research and Technology Development Fund JPMEERF20192005 of the Environmental Restoration and Conservation Agency of Japan, the MEXT-Program for the Advanced Studies of Climate Change Projection (SENTAN) Grant JPMXD0722680734, and the Integrated Research Program for Advancing Climate Models (TOUGOU) Grant JPMXD0717935457 from the Ministry of Education, Culture, Sports, Science, and Technology (MEXT), by JSPS KAKENHI grants (18H03819 and 19H00963), and by the Research Field of Hokkaido Weather Forecast and Technology Development (endowed by Hokkaido Weather Technology Center Co., Ltd.).

*Data availability statement.* The MRI-AGCM and NHRCM20 d4PDF datasets can be downloaded from the Data Integration and Analysis System Program (DIAS; https://diasjp.net/en/). The NHRCM05 d4PDF ensemble simulation can be provided upon request. The BestTrack data can be found online (https://www.jma.go.jp/jma/jma-eng/jma-center/rsmc-hp-pub-eg/besttrack.html; JMA 2013). The ERA5 data were downloaded from the Copernicus Climate Change Service (https://cds.climate.copernicus.eu/; Copernicus Climate Change Service 2017). The JRA-55 data were downloaded from the Research Data Archive at the National Center for Atmospheric Research Computational and Information Systems Laboratory (https://rda.ucar.edu/). The Radar/Rain Gauge-Analyzed Precipitation (RA) dataset was purchased from the Japan Meteorological Business Support Center (http://www.jmbsc.or.jp/jp/offline/cd0100.html).

## REFERENCES

Adachi, S., and F. Kimura, 2007: A 36-year climatology of surface cyclogenesis in East Asia using high-resolution reanalysis data. *SOLA*, **3**, 113–116, https://doi.org/10.2151/sola.2007-029.

Barcikowska, M., F. Feser, W. Zhang, and W. Mei, 2017: Changes in intense tropical cyclone activity for the western North Pacific during the last decades derived from a regional climate model simulation. *Climate Dyn.*, **49**, 2931–2949, https://doi.org/10.1007/s00382-016-3420-0.

Bengtsson, L., K. I. Hodges, and N. Keenlyside, 2009: Will extratropical storms intensify in a warmer climate? *J. Climate*, **22**, 2276–2301, https://doi.org/10.1175/2008JCLI2678.1.

Catto, J. L., L. C. Shaffrey, and K. I. Hodges, 2010: Can climate models capture the structure of extratropical cyclones? *J. Climate*, **23**, 1621–1635, https://doi.org/10.1175/2009JCLI3318.1.

——, and Coauthors, 2019: The future of midlatitude cyclones. *Curr. Climate Change Rep.*, **5**, 407–420, https://doi.org/10.1007/s40641-019-00149-4.

Chan, K. T. F., 2019: Are global tropical cyclones moving slower in a warming climate? *Environ. Res. Lett.*, **14**, 104015, https://doi.org/10.1088/1748-9326/ab4031.

——, and J. C. L. Chan, 2015: Impacts of vortex intensity and outer winds on tropical cyclone size. *Quart. J. Roy. Meteor. Soc.*, **141**, 525–537, https://doi.org/10.1002/qj.2374.

Copernicus Climate Change Service, 2017: ERA5: Fifth generation of ECMWF atmospheric reanalyses of the global climate. Copernicus Climate Change Service Climate Data Store (CDS), accessed 1 November 2021, https://cds.climate.copernicus.eu/#!/search?text=ERA5&type=dataset.

Emori, S., and S. J. Brown, 2005: Dynamic and thermodynamic changes in mean and extreme precipitation under changed climate. *Geophys. Res. Lett.*, **32**, L17706, https://doi.org/10.1029/2005GL023272.

Finnis, J., M. M. Holland, M. C. Serreze, and J. J. Cassano, 2007: Response of Northern Hemisphere extratropical cyclone activity and associated precipitation to climate change, as represented by the Community Climate System Model. *J. Geophys. Res.*, **112**, G04S42, https://doi.org/10.1029/2006JG000286.

Frank, W. M., and E. A. Ritchie, 2001: Effects of vertical wind shear on the intensity and structure of numerically simulated hurricanes. *Mon. Wea. Rev.*, **129**, 2249–2269, https://doi.org/10.1175/1520-0493(2001)129<2249:EOVWSO>2.0.CO;2.

Gutmann, E. D., and Coauthors, 2018: Changes in hurricanes from a 13-yr convection-permitting pseudo–global warming simulation. *J. Climate*, **31**, 3643–3657, https://doi.org/10.1175/JCLI-D-17-0391.1.

Harada, Y., and Coauthors, 2016: The JRA-55 reanalysis: Representation of atmospheric circulation and climate variability. *J. Meteor. Soc. Japan*, **94**, 269–302, https://doi.org/10.2151/jmsj.2016-015.

Hasegawa, A., and S. Emori, 2007: Effect of air-sea coupling in the assessment of $CO_2$-induced intensification of tropical cyclone activity. *Geophys. Res. Lett.*, **34**, L05701, https://doi.org/10.1029/2006GL028275.

Hatsuzuka, D., and T. Sato, 2019: Future changes in monthly extreme precipitation in Japan using large-ensemble regional climate simulations. *J. Hydrometeor.*, **20**, 563–574, https://doi.org/10.1175/JHM-D-18-0095.1.

—— and ——, 2022: Impact of SST on present and future extreme precipitation in Hokkaido investigated considering weather patterns. *J. Geophys. Res. Atmos.*, **127**, e2021JD036120, https://doi.org/10.1029/2021JD036120.

Hawcroft, M. K., L. C. Shaffrey, K. I. Hodges, and H. F. Dacre, 2012: How much Northern Hemisphere precipitation is associated with extratropical cyclones? *Geophys. Res. Lett.*, **39**, L24809, https://doi.org/10.1029/2012GL053866.

——, E. Walsh, K. Hodges, and G. Zappa, 2018: Significantly increased extreme precipitation expected in Europe and North America from extratropical cyclones. *Environ. Res. Lett.*, **13**, 124006, https://doi.org/10.1088/1748-9326/aaed59.

He, C., and T. Zhou, 2015: Responses of the western North Pacific subtropical high to global warming under RCP4.5 and RCP8.5 scenarios projected by 33 CMIP5 models: The dominance of tropical Indian Ocean–tropical western Pacific SST gradient. *J. Climate*, **28**, 365–380, https://doi.org/10.1175/JCLI-D-13-00494.1.

——, ——, A. Lin, B. Wu, D. Gu, C. Li, and B. Zhang, 2015: Enhanced or weakened western North Pacific subtropical high under global warming? *Sci. Rep.*, **5**, 16771, https://doi.org/10.1038/srep16771.

Hersbach, H., and Coauthors, 2020: The ERA5 global reanalysis. *Quart. J. Roy. Meteor. Soc.*, **146**, 1999–2049, https://doi.org/10.1002/qj.3803.

Hirahara, S., H. Ohno, Y. Oikawa, and S. Maeda, 2012: Strengthening of the southern side of the jet stream and delayed withdrawal of baiu season in future climate. *J. Meteor. Soc. Japan*, **90**, 663–671, https://doi.org/10.2151/jmsj.2012-506.

——, M. Ishii, and Y. Fukuda, 2014: Centennial-scale sea surface temperature analysis and its uncertainty. *J. Climate*, **27**, 57–75, https://doi.org/10.1175/JCLI-D-12-00837.1.

Hoshino, T., T. J. Yamada, and H. Kawase, 2020: Evaluation for characteristics of tropical cyclone induced heavy rainfall over the sub-basins in the central Hokkaido, northern Japan by 5-km large ensemble experiments. *Atmosphere*, **11**, 435, https://doi.org/10.3390/atmos11050435.

Iizumi, T., and Coauthors, 2012: Future change of daily precipitation indices in Japan: A stochastic weather generator-based bootstrap approach to provide probabilistic climate information. *J. Geophys. Res.*, **117**, D11114, https://doi.org/10.1029/2011JD017197.

Inatsu, M., 2009: The neighbor enclosed area tracking algorithm for extratropical wintertime cyclones. *Atmos. Sci. Lett.*, **10**, 267–272, https://doi.org/10.1002/asl.238.

——, T. Sato, T. J. Yamada, R. Kuno, S. Sugimoto, M. A. Farukh, Y. N. Pokhrel, and S. Kure, 2015: Multi-GCM by multi-RAM experiments for dynamical downscaling on summertime climate change in Hokkaido. *Atmos. Sci. Lett.*, **16**, 297–304, https://doi.org/10.1002/asl2.557.

Ishii, M., and N. Mori, 2020: d4PDF: Large-ensemble and high-resolution climate simulations for global warming risk assessment. *Prog. Earth Planet. Sci.*, **7**, 58, https://doi.org/10.1186/s40645-020-00367-7.

Ishizaki, H., and H. Matsuyama, 2018: Distribution of the annual precipitation ratio of radar/raingauge-analyzed precipitation to AMeDAS across Japan. *SOLA*, **14**, 192–196, https://doi.org/10.2151/sola.2018-034.

Ito, R., T. Takemi, and O. Arakawa, 2016: A possible reduction in the severity of typhoon wind in the northern part of Japan under global warming: A case study. *SOLA*, **12**, 100–105, https://doi.org/10.2151/sola.2016-023.

JMA, 2013: JRA-55: Japanese 55-Year Reanalysis, daily 3-hourly and 6-hourly data. National Center for Atmospheric Research Computational and Information Systems Laboratory Research Data Archive, accessed 1 November 2021, https://doi.org/10.5065/D6HH6H41.

Jones, P. W., 1999: First- and second-order conservative remapping schemes for grids in spherical coordinates. *Mon. Wea. Rev.*, **127**, 2204–2210, https://doi.org/10.1175/1520-0493(1999)127<2204:FASOCR>2.0.CO;2.

Kamahori, H., N. Yamazaki, N. Mannoji, and K. Takahashi, 2006: Variability in intense tropical cyclone days in the western North Pacific. *SOLA*, **2**, 104–107, https://doi.org/10.2151/sola.2006-027.

Kanada, S., K. Tsuboki, H. Aiki, S. Tsujino, and I. Takayabu, 2017a: Future enhancement of heavy rainfall events associated with a typhoon in midlatitude regions. *SOLA*, **13**, 246–251, https://doi.org/10.2151/sola.2017-045.

——, T. Takemi, M. Kato, S. Yamazaki, H. Fudeyasu, K. Tsuboki, O. Arakawa, and I. Takayabu, 2017b: A multimodel intercomparison of an intense typhoon in future, warmer climates by four 5-km-mesh models. *J. Climate*, **30**, 6017–6036, https://doi.org/10.1175/JCLI-D-16-0715.1.

——, K. Tsuboki, and I. Takayabu, 2020: Future changes of tropical cyclones in the midlatitudes in 4-km-mesh downscaling experiments from large-ensemble simulations. *SOLA*, **16**, 57–63, https://doi.org/10.2151/sola.2020-010.

Kawazoe, S., and W. J. Gutowski Jr., 2018: Evaluation of regional very heavy precipitation events during the summer season using NARCCAP contemporary simulations. *Int. J. Climatol.*, **38** (Suppl. 1), e832–e846, https://doi.org/10.1002/joc.5412.

Kim, H.-S., G. A. Vecchi, T. R. Knutson, W. G. Anderson, T. L. Delworth, A. Rosati, F. Zeng, and M. Zhao, 2014: Tropical cyclone simulation and response to $CO_2$ doubling in the GFDL CM2.5 high-resolution coupled climate model. *J. Climate*, **27**, 8034–8054, https://doi.org/10.1175/JCLI-D-13-00475.1.

Kimoto, M., N. Yasutomi, C. Yokoyama, and S. Emori, 2005: Projected changes in precipitation characteristics around Japan under the global warming. *SOLA*, **1**, 85–-88, https://doi.org/10.2151/sola.2005-023.

Kitabatake, N., 2011: Climatology of extratropical transition of tropical cyclones in the western North Pacific defined by using cyclone phase space. *J. Meteor. Soc. Japan*, **89**, 309–325, https://doi.org/10.2151/jmsj.2011-402.

Kitano, Y., T. Yamamoto, A. Kobayashi, and T. J. Yamada, 2017: Statistical analysis of typhoon related events in Hokkaido and surroundings in the last 56 years including the 2016 heavy rainfall (in Japanese). *J. Japan Soc. Civ. Eng.*, **73**, I_1231–I_1236, https://doi.org/10.2208/jscejhe.73.I_1231.

Klotzbach, P. J., M. M. Bell, S. G. Bowen, E. I. Gibney, K. R. Knapp, and C. J. Schreck III, 2020: Surface pressure a more skillful predictor of normalized hurricane damage than maximum wind. *Bull. Amer. Meteor. Soc.*, **101**, E830–E846, https://doi.org/10.1175/BAMS-D-19-0062.1.

Knutson, T. R., J. J. Sirutis, M. Zhao, R. E. Tuleya, M. Bender, G. A. Vecchi, G. Villarini, and D. Chavas, 2015: Global projection of intense tropical cyclone activity for the late twenty-first century from dynamical downscaling of CMIP5/RCP4.5 scenarios. *J. Climate*, **28**, 7203–7224, https://doi.org/10.1175/JCLI-D-15-0129.1.

——, and Coauthors, 2020: Tropical cyclones and climate change assessment: Part II: Projected response to anthropogenic warming. *Bull. Amer. Meteor. Soc.*, **101**, E303–E322, https://doi.org/10.1175/BAMS-D-18-0194.1.

Kobayashi, S., and Coauthors, 2015: The JRA-55 reanalysis: General specifications and basic characteristics. *J. Meteor. Soc. Japan*, **93**, 5–48, https://doi.org/10.2151/jmsj.2015-001.

Kodama, C., B. Stevens, T. Mauritsen, T. Seiki, and M. Satoh, 2019: A new perspective for future precipitation change from intense extratropical cyclones. *Geophys. Res. Lett.*, **46**, 12 435–12 444, https://doi.org/10.1029/2019GL084001.

Kossin, J. P., 2018: A global slowdown of tropical-cyclone translation speed. *Nature*, **558**, 104–107, https://doi.org/10.1038/s41586-018-0158-3.

——, and C. S. Velden, 2004: A pronounced bias in tropical cyclone minimum sea level pressure estimation based on the Dvorak technique. *Mon. Wea. Rev.*, **132**, 165–173, https://doi.org/10.1175/1520-0493(2004)132<0165:APBITC>2.0.CO;2.

Lee, J., S.-W. Son, H.-O. Cho, J. Kim, D.-H. Cha, J. R. Gyakum, and D. Chen, 2020: Extratropical cyclones over East Asia: Climatology, seasonal cycle, and long-term trend. *Climate Dyn.*, **54**, 1131–1144, https://doi.org/10.1007/s00382-019-05048-w.

McDonald, R. E., 2011: Understanding the impact of climate change on Northern Hemisphere extra-tropical cyclones. *Climate Dyn.*, **37**, 1399–1425, https://doi.org/10.1007/s00382-010-0916-x.

Michaelis, A. C., J. Willison, G. M. Lackmann, and W. A. Robinson, 2017: Changes in winter North Atlantic extratropical cyclones in high-resolution regional pseudo–global warming simulations. *J. Climate*, **30**, 6905–6925, https://doi.org/10.1175/JCLI-D-16-0697.1.

Miyasaka, T., H. Kawase, T. Nakaegawa, Y. Imada, and I. Takayabu, 2020: Future projection of heavy precipitation in Kanto and associated weather patterns using large ensemble high-resolution simulations. *SOLA*, **16**, 125–131, https://doi.org/10.2151/sola.2020-022.

Mizuta, R., and Coauthors, 2012: Climate simulations using MRI AGCM3.2 with 20-km grid. *J. Meteor. Soc. Japan*, **90A**, 233–258, https://doi.org/10.2151/jmsj.2012-A12.

——, O. Arakawa, T. Ose, S. Kusunoki, H. Endo, and A. Kitoh, 2014: Classification of CMIP5 future climate responses by the tropical sea surface temperature changes. *SOLA*, **10**, 167–171, https://doi.org/10.2151/sola.2014-035.

——, and Coauthors, 2017: Over 5000 years of ensemble future climate simulations by 60 km global and 20 km regional atmospheric models. *Bull. Amer. Meteor. Soc.*, **98**, 1383–1398, https://doi.org/10.1175/BAMS-D-16-0099.1.

Moon, I.-J., S.-H. Kim, and J. C. L. Chan, 2019: Climate change and tropical cyclone trend. *Nature*, **570**, E3–E5, https://doi.org/10.1038/s41586-019-1222-3.

Murakami, H., B. Wang, and A. Kitoh, 2011: Future changes of western North Pacific typhoons: Projections by a 20-km-mesh global atmospheric model. *J. Climate*, **24**, 1154–1169, https://doi.org/10.1175/2010JCLI3723.1.

——, and Coauthors, 2012: Future changes in tropical cyclone activity projected by the new high-resolution MRI-AGCM. *J. Climate*, **25**, 3237–3260, https://doi.org/10.1175/JCLI-D-11-00415.1.

Nayak, S., and T. Takemi, 2020a: Typhoon-induced precipitation characterization over northern Japan: A case study for typhoons in 2016. *Prog. Earth Planet. Sci.*, **7**, 39, https://doi.org/10.1186/s40645-020-00347-x.

——, and ——, 2020b: Robust responses of typhoon hazards in northern Japan to global warming climate: Cases of landfalling typhoons in 2016. *Meteor. Appl.*, **27**, e1954, https://doi.org/10.1002/met.1954.

NOAA/National Geophysical Data Center, 2006: 2-minute Gridded Global Relief Data (ETOPO2) v2. NOAA National Centers for Environmental Information, accessed 28 June 2019, https://doi.org/10.7289/V5J1012Q.

Ogata, T., R. Mizuta, Y. Adachi, H. Murakami, and T. Ose, 2016: Atmosphere-ocean coupling effect on intense tropical cyclone distribution and its future change with 60 km-AOGCM. *Sci. Rep.*, **6**, 29800, https://doi.org/10.1038/srep29800.

Oouchi, K., J. Yoshimura, H. Yoshimura, R. Mizuta, S. Kusunoki, and A. Noda, 2006: Tropical cyclone climatology in a global-warming climate as simulated in a 20 km-mesh global atmospheric model: Frequency and wind intensity analyses. *J. Meteor. Soc. Japan*, **84**, 259–276, https://doi.org/10.2151/jmsj.84.259.

Ose, T., Y. Takaya, S. Maeda, and T. Nakaegawa, 2020: Resolution of summertime East Asian pressure patterns and southerly monsoon wind in the CMIP5 multi-model future projections. *J. Meteor. Soc. Japan*, **98**, 927–944, https://doi.org/10.2151/jmsj.2020-047.

Paterson, L. A., B. N. Hanstrum, N. E. Davidson, and H. C. Weber, 2005: Influence of environmental vertical wind shear on the intensity of hurricane-strength tropical cyclones in the Australian Region. *Mon. Wea. Rev.*, **133**, 3644–3660, https://doi.org/10.1175/MWR3041.1.

Pfahl, S., and H. Wernli, 2012: Quantifying the relevance of cyclones for precipitation extremes. *J. Climate*, **25**, 6770–6780, https://doi.org/10.1175/JCLI-D-11-00705.1.

——, and M. Sprenger, 2016: On the relationship between extratropical cyclone precipitation and intensity. *Geophys. Res. Lett.*, **43**, 1752–1758, https://doi.org/10.1002/2016GL068018.

Powell, M. D., and T. A. Reinhold, 2007: Tropical cyclone destructive potential by integrated kinetic energy. *Bull. Amer. Meteor. Soc.*, **88**, 513–526, https://doi.org/10.1175/BAMS-88-4-513.

Priestley, M. D. K., and J. L. Catto, 2022: Future changes in the extratropical storm tracks and cyclone intensity, wind speed, and structure. *Wea. Climate Dyn.*, **3**, 337–360, https://doi.org/10.5194/wcd-3-337-2022.

Sasaki, H., A. Murata, M. Hanafusa, M. Oh'izumi, and K. Kurihara, 2011: Reproducibility of present climate in a non-hydrostatic regional climate model nested within an atmosphere general circulation model. *SOLA*, **7**, 173–176, https://doi.org/10.2151/sola.2011-044.

Satake, Y., M. Inatsu, M. Mori, and A. Hasegawa, 2013: Tropical cyclone tracking using a neighbor enclosed area tracking algorithm. *Mon. Wea. Rev.*, **141**, 3539–3555, https://doi.org/10.1175/MWR-D-12-00092.1.

Simmonds, I., 2000: Size changes over the life of sea level cyclones in the NCEP reanalysis. *Mon. Wea. Rev.*, **128**, 4118–4125, https://doi.org/10.1175/1520-0493(2000)129<4118:SCOTLO>2.0.CO;2.

Sinclair, V. A., M. Rantanen, P. Haapanala, J. Raisanen, and H. Jarvinen, 2020: The characteristics and structure of extratropical cyclones in a warmer climate. *Wea. Climate Dyn.*, **1** (1), 1–25, https://doi.org/10.5194/wcd-1-1-2020.

Sun, Y., and Coauthors, 2017: Impact of ocean warming on tropical cyclone size and its destructiveness. *Sci. Rep.*, **7**, 8154, https://doi.org/10.1038/s41598-017-08533-6.

Takabatake, D., and M. Inatsu, 2022: Summertime precipitation in Hokkaido and Kyushu, Japan in response to global warming. *Climate Dyn.*, **58**, 1671–1682, https://doi.org/10.1007/s00382-021-05983-7.

Tamaki, Y., M. Inatsu, D. Nguyen-Le, and T. J. Yamada, 2018: Heavy rainfall duration bias in dynamical downscaling and its related synoptic patterns in summertime Asian monsoon. *J. Appl. Meteor. Climatol.*, **57**, 1477–1496, https://doi.org/10.1175/JAMC-D-17-0116.1.

Tsuboki, K., M. K. Yoshioka, T. Shinoda, M. Kato, S. Kanada, and A. Kitoh, 2015: Future increase of supertyphoon intensity associated with climate change. *Geophys. Res. Lett.*, **42**, 646–652, https://doi.org/10.1002/2014GL061793.

Ulbrich, U., G. C. Leckenbusch, and J. G. Pinto, 2009: Extra-tropical cyclones in the present the future climate: A review. *Theor. Appl. Climatol.*, **96**, 117–131, https://doi.org/10.1007/s00704-008-0083-8.

Utsumi, N., S. Seto, S. Kanae, E. E. Maeda, and T. Oki, 2011: Does higher surface temperature intensity extreme precipitation? *Geophys. Res. Lett.*, **38**, L16708, https://doi.org/10.1029/2011GL048426.

——, H. Kim, S. Kanae, and T. Oki, 2017: Relative contribution of weather systems to mean and extreme global precipitation. *J. Geophys. Res. Atmos.*, **122**, 152–167, https://doi.org/10.1002/2016JD025222.

Wang, C., L. Wu, J. Lu, Q. Liu, H. Zhao, W. Tian, and J. Cao, 2020: Interannual variability of the basinwide translation speed of tropical cyclones in the western North Pacific. *J. Climate*, **33**, 8641–8650, https://doi.org/10.1175/JCLI-D-19-0995.1.

Watanabe, M., and Coauthors, 2010: Improved climate simulation by MIROC5: Mean states, variability, and climate sensitivity. *J. Climate*, **23**, 6312–6335, https://doi.org/10.1175/2010JCLI3679.1.

Watanabe, S.-I., A. Murata, H. Sasaki, H. Kawase, and M. Nosaka, 2019: Future projection of tropical cyclone precipitation over Japan with a high-resolution regional climate model. *J. Meteor. Soc. Japan*, **97**, 805–820, https://doi.org/10.2151/jmsj.2019-045.

Watterson, I. G., 2006: The intensity of precipitation during extra-tropical cyclones in global warming simulations: A link to cyclone intensity? *Tellus*, **58A**, 82–97, https://doi.org/10.1111/j.1600-0870.2006.00147.x.

Wu, L., W. Tian, Q. Liu, J. Cao, and J. A. Knaff, 2015: Implication of the observed relationship between tropical cyclone size and intensity over the western North Pacific. *J. Climate*, **28**, 9501–9506, https://doi.org/10.1175/JCLI-D-15-0628.1.

Yamada, T. J., M. A. Farukh, T. Fukushima, M. Inatsu, T. Sato, Y. N. Pokhrel, and T. Oki, 2014: Extreme precipitation intensity in future climates associated with the Clausius-Clapeyron-like relationship. *Hydrol. Res. Lett.*, **8**, 108–113, https://doi.org/10.3178/hrl.8.108.

——, T. Hoshino, and A. Suzuki, 2021: Using a massive high-resolution ensemble climate data set to examine dynamic and thermodynamic aspects of heavy precipitation change. *Atmos. Sci. Lett.*, **22**, e1065, https://doi.org/10.1002/asl.1065.

Yamada, Y., M. Satoh, M. Sugi, C. Kodama, A. T. Noda, M. Nakano, and T. Nasuno, 2017: Response of tropical cyclone activity and structure to global warming in a high-resolution global nonhydrostatic model. *J. Climate*, **30**, 9703–9724, https://doi.org/10.1175/JCLI-D-17-0068.1.

Yamaguchi, M., and S. Maeda, 2020: Slowdown of typhoon translation speeds in mid-latitudes in September influenced by Pacific decadal oscillation and global warming. *J. Meteor. Soc. Japan*, **98**, 1321–1334, https://doi.org/10.2151/jmsj.2020-068.

——, J. C. L. Chan, I.-J. Moon, K. Yoshida, and R. Mizuta, 2020: Global warming changes tropical cyclone translation speed. *Nat. Commun.*, **11**, 47, https://doi.org/10.1038/s41467-019-13902-y.

Yamamoto, M., T. Ohigashi, K. Tsuboki, and N. Hirose, 2011: Cloud-resolving simulation of heavy snowfalls in Japan for late December 2005: Application of ocean data assimilation to a snow disaster. *Nat. Hazards Earth Syst. Sci.*, **11**, 2555–2565, https://doi.org/10.5194/nhess-11-2555-2011.

Yasuda, T., H. Mase, and N. Mori, 2010: Projection of future typhoons landing on Japan based on stochastic typhoon model utilizing AGCM projections. *Hydrol. Res. Lett.*, **4**, 65–69, https://doi.org/10.3178/hrl.4.65.

Yettella, V., and J. E. Kay, 2017: How will precipitation change in extratropical cyclones as the planet warms? Insight from a large initial condition climate model ensemble. *Climate Dyn.*, **49**, 1765–1781, https://doi.org/10.1007/s00382-016-3410-2.

Yoshida, A., and Y. Asuma, 2004: Structures and environment of explosively developing extratropical cyclones in the northwestern Pacific region. *Mon. Wea. Rev.*, **132**, 1121–1142, https://doi.org/10.1175/1520-0493(2004)132<1121:SAEOED>2.0.CO;2.

Yoshida, K., M. Sugi, R. Mizuta, H. Murakami, and M. Ishii, 2017: Future changes in tropical cyclone activity in high-resolution large-ensemble simulations. *Geophys. Res. Lett.*, **44**, 9910–9917, https://doi.org/10.1002/2017GL075058.

Zhang, D., H. Zhang, J. Zheng, X. Cheng, D. Tian, and D. Chen, 2020: Changes in tropical-cyclone translation speed over the western North Pacific. *Atmosphere*, **11**, 93, https://doi.org/10.3390/atmos11010093.

Zhou, T., and Coauthors, 2009: Why the western Pacific subtropical high has extended westward since the late 1970s. *J. Climate*, **22**, 2199–2215, https://doi.org/10.1175/2008JCLI2527.1.